Dynamical control of qubit coherence: Random versus deterministic schemes

Lea F. Santos* and Lorenza Viola†

Department of Physics and Astronomy, Dartmouth College, 6127 Wilder Laboratory, Hanover, New Hampshire 03755, USA
(Received 5 August 2005; published 5 December 2005)

We reexamine the problem of switching off unwanted phase evolution and decoherence in a single two-state quantum system in the light of recent results on random dynamical decoupling methods [L. Viola and E. Knill, Phys. Rev. Lett. **94**, 060502 (2005)]. A systematic comparison with standard cyclic decoupling is effected for a variety of dynamical regimes, including the case of both semiclassical and fully quantum decoherence models. In particular, exact analytical expressions are derived for randomized control of decoherence from a bosonic environment. We investigate quantitatively control protocols based on purely deterministic, purely random, as well as hybrid design, and identify their relative merits and weaknesses at improving system performance. We find that for time-independent systems, hybrid protocols tend to perform better than pure random and may improve over standard asymmetric schemes, whereas random protocols can be considerably more stable against fluctuations in the system parameters. Beside shedding light on the physical requirements underlying randomized control, our analysis further demonstrates the potential for explicit control settings where the latter may significantly improve over conventional schemes.

PACS number(s): 03.67.Pp, 03.65.Yz, 05.40.Ca, 89.70.+c

I. INTRODUCTION

The design and characterization of strategies for controlling quantum dynamics is vital to a broad spectrum of applications within contemporary physics and engineering. These range from traditional coherent-control settings like high-resolution nuclear [1,2] and molecular spectroscopy [3] to a variety of tasks motivated by the rapidly growing field of quantum information science [4]. In particular, the ability to counteract decoherence effects that unavoidably arise in the dynamics of a real-world quantum system coupled to its surrounding environment is a prerequisite for scalable realizations of quantum-information processing (QIP), as actively pursued through a variety of proposed quantum device technologies [5].

Active decoupling techniques offer a conceptually simple yet powerful control-theoretic setting for quantum-dynamical engineering of both closed-system (unitary) and open-system (nonunitary) evolutions. Inspired by the idea of *coherent averaging* of interactions by means of tailored pulse sequences in nuclear magnetic resonance (NMR) spectroscopy [6], decoupling protocols consist of repetitive sequences of control operations (typically drawn from a finite repertoire), whose net effect is to coherently modify the natural target dynamics to a desired one. In practice, a critical decoupling task is the selective removal of unwanted couplings between subsystems of a fully or partially controllable composite quantum system. Historically, a prototype example is the elimination of unwanted phase evolution in interacting spin systems via trains of π pulses (the so-called Hahn-echo and Carr-Purcell sequences [7,8]). For open quantum systems, this line of reasoning motivates the question of whether removing the coupling between the system of interest and its environment

may be feasible by a control action restricted to the former only. Such a question was addressed in [9] for the paradigmatic case of a single qubit coupled to a bosonic reservoir, establishing the possibility of decoherence suppression in the limit of rapid spin flipping via the echo sequence mentioned above.

The study of dynamical decoupling as a general strategy for quantum coherent and error control has since then attracted a growing interest from the point of view of both model-independent decoupling design and optimization and the application to specific physical systems. Representative contributions include the extension to arbitrary finite-dimensional systems via dynamical-algebraic [10,11], geometric [12], and linear-algebraic [13] formulations; the construction of fault-tolerant Eulerian [14] and concatenated decoupling protocols [15], as well as efficient combinatorial schemes [16–19]; the connection with quantum Zeno physics [20]; proposed applications to the compensation of specific decoherence mechanisms (notably, magnetic-state decoherence [21] and $1/f$ noise [22–26]) and/or the removal of unwanted evolution within trapped-ion [27,28] and solid-state quantum computing architectures [29]. These theoretical advances have been paralleled by steady experimental progress. Beginning with a proof-of-principle demonstration of decoherence suppression in a single-photon polarization interferometer [30], dynamical decoupling techniques have been implemented alone and in conjunction with quantum error correction within liquid-state NMR QIP [31,32] and have inspired charge-based [33] and flux-based [34] echo experiments in superconducting qubits. Recently, dynamic decoherence control of a solid-state nuclear quadrupole qubit has been reported [35].

All the formulations of dynamical decoupling mentioned so far share the feature of involving purely *deterministic* control actions. In the simplest setting, these are arbitrarily strong, effectively instantaneous rotations (so-called *bang-bang controls*) chosen from a discrete group $\mathcal{G}$. Decoupling according to $\mathcal{G}$ is then accomplished by sequentially cycling

---

*Electronic address: Lea.F.Dos.Santos@Dartmouth.edu
†Electronic address: Lorenza.Viola@Dartmouth.edu

the control propagator through *all* the elements of $\mathcal{G}$. If Δt denotes the separation between consecutive control operations, this translates into a minimal averaging time scale $T_c = |\mathcal{G}| \Delta t$ of length proportional to the size $|\mathcal{G}|$ of $\mathcal{G}$.

The exploration of decoupling schemes incorporating *stochastic* control actions was only recently undertaken. A general control-theoretic framework was introduced by Viola and Knill in [36] (see also [37]), based on the idea of seeking faster convergence (with respect to an appropriately defined metric) by *randomly sampling* rather than systematically implementing control operations from $\mathcal{G}$. Based on general lower bounds for pure-state error probabilities, the analysis of [36] indicated that random schemes could outperform their cyclic counterpart in situations where a large number of elementary control operations is required or, even for small control groups, when the interactions to be removed vary themselves in time over time scales long compared to Δt but short compared to T_c. Furthermore, it also suggested that advantageous features of pure cyclic and random methods could be enhanced by appropriately merging protocols within a hybrid design. The usefulness of randomization in the context of actively suppressing *coherent* errors due to residual static interactions was meanwhile independently demonstrated by the so-called *Pauli random error correction* (PAREC) method, followed by the more recent *embedded dynamical decoupling* method—both due to Kern and co-workers [38,39]. Both protocols may be conceptually understood as following from randomization over the Pauli group $\mathcal{G}_P = \{\mathbb{1}, \sigma_x, \sigma_y, \sigma_z\}$, used alone or, respectively, in conjunction with a second set of deterministic control operations.

Our goal in this work is twofold: first, to develop a quantitative understanding of *typical* randomized control performance for both *coherent and decoherent phase errors*, beginning from the simplest scenario of a single qubit already investigated in detail in the deterministic case [9]; second, to clarify the *physical* picture underlying random control, by devoting, in particular, special attention to elucidate the control action and requirements in rotating frames associated with different dynamical representations. The fact that the controlled dynamics remains exactly solvable in the bang-bang (BB) limit makes the single-qubit pure-dephasing setting an ideal test bed for these purposes. From a general standpoint, since spin-flip decoupling corresponds to averaging over the smallest (nontrivial) group $\mathcal{Z}_2 = \{0, 1\}$, with $T_c = 2\Delta t$ [10,11], this system is not yet expected to show the full advantage of the random approach. Remarkably, however, control scenarios can still be identified, where randomized protocols indeed represent the most suitable choice.

The content of the paper is organized as follows. After laying out the relevant system and control settings in Sec. II, we begin the comparison between cyclic and randomized protocols by studying the task of phase refocusing in a qubit evolving unitarily in Sec. III. Control of decoherence from purely dephasing semiclassical and quantum environments is investigated in the main part of the paper, Secs. IV and V. We focus on the relevant situations of decoherence due to random telegraph noise and to a fully quantum bosonic bath, respectively. Both exact analytical and numerical results for the controlled decoherence process are presented in the latter case. We summarize our results and discuss their significance

from the broader perspective of constructively exploiting randomness in physical systems in Sec. VI, by also pointing to some directions for future research. Additional technical considerations are included in a separate appendix.

II. SINGLE-QUBIT QUANTUM-CONTROL SETTINGS

Our target system S is a single qubit, residing on a state space $\mathcal{H}_S \simeq \mathbb{C}^2$. The influence of the surrounding environment may be formally accounted for by two main modifications to the isolated qubit dynamics. First, S may couple to effectively *classical* degrees of freedom, whose net effect may be modeled through a deterministic or random time-dependent modification of the system parameters. Additionally, S may couple to a *quantum* environment E; that is, a second quantum system defined on a state space $\mathcal{H}_E$ with which S may become entangled in the course of the evolution. For the present purposes, E will be schematized as a bosonic reservoir consisting of independent harmonic modes. Let $\mathbb{1}_{S,E}$ denote the identity operator on $\mathcal{H}_{S,E}$, respectively. Throughout the paper, we will consider different dynamical scenarios, corresponding to special cases of the following total drift Hamiltonian on $\mathcal{H}_S \otimes \mathcal{H}_E$:

$$H_0(t) = H_S(t) \otimes \mathbb{1}_E + \mathbb{1}_S \otimes H_E + H_{SE}(t), \quad (1)$$

where

$$H_S(t) = \frac{\omega_0(t)}{2} \sigma_z,$$

$$H_E = \sum_k \omega_k b_k^\dagger b_k,$$

$$H_{SE}(t) = \mu \sigma_z \otimes \sum_k [g_k(t) b_k^\dagger + g_k^*(t) b_k]. \quad (2)$$

Here, we set $\hbar = 1$, and σ_i $(i = x, y, z)$, $b_k^\dagger$, and b_k denote Pauli spin matrices and canonical creation and annihilation bosonic operators of the kth environmental mode with frequency ω_k, respectively. $\omega_0(t)$ and $g_k(t)$ are real and complex functions that account for an effectively time-dependent frequency of the system and its coupling to the kth reservoir mode, respectively. We shall write

$$\omega_0(t) = \omega_0 + \delta\omega_0(t),$$

$$g_k(t) = g_k + \delta g_k(t), \quad (3)$$

for an appropriate choice of central values ω_0, g_k and modulation functions $\delta\omega_0$, δg_k, respectively. The adimensional parameter μ is introduced for notational convenience, allowing us to include $(\mu = 1)$ or not $(\mu = 0)$ the coupling to E as desired. Physically, because $H_S(t)$ and $H_{SE}(t)$ commute at all times, the above Hamiltonian describes a *purely decohering* coupling between S and E, which does not entail energy exchange. While in general dissipation might also occur, focusing on pure decoherence is typically justified for sufficiently short time scales [40,41] and, as we shall see, has the advantage of making exact solutions available as benchmarks.

Control is introduced by adjoining a classical controller acting on S—that is, by adding a time-dependent term to the above target Hamiltonian,

$$H_0(t) \mapsto H_0(t) + H_c(t) \otimes \mathbb{1}_E. \qquad (4)$$

In our case, $H_c(t)$ will be designed so as to implement appropriate sequences of BB pulses. This may be accomplished by starting from a rotating radiofrequency field (or, upon invoking the rotating-wave approximation, by a linearly polarized oscillating field), described by the following amplitude- and phase-modulated Hamiltonian:

$$H_c(t) = \sum_j V^{(j)}(t)\{\cos[\omega t + \varphi_j(t)]\sigma_x + \sin[\omega t + \varphi_j(t)]\sigma_y\},$$

with

$$V^{(j)}(t) = V[\Theta(t - t_j) - \Theta(t - t_j - \tau)].$$

Here, $\Theta(\cdot)$ denotes the Heaviside step function [defined as $\Theta(x)=0$ for $x \leq 0$ and $\Theta=1$ for $x>0$], V and τ are positive parameters, and t_j denotes the instants at which the pulses are applied. If the carrier frequency is tuned on resonance with the central frequency, $\omega=\omega_0$, and the phase $\varphi_j(t)=-\omega_0 t_j$ for each j, the above Hamiltonian schematizes a train of *identical* control pulses of amplitude V and duration τ in the physical frame. Under the BB requirement of impulsive switching ($\tau \to 0$) with unbounded strength ($V \to \infty$), it is legitimate to neglect $H_0(t)$ (including possible off-resonant effects) within each pulse, effectively leading to qubit rotations about the $\hat{x}$ axis. In particular, a π rotation corresponds to $2V\tau = \pm\pi$ (see also the Appendix).

In what follows, we shall focus on using trains of BB π pulses to effectively achieve a net evolution characterized by the identity operator (the so-called *no-op* gate). This requires averaging unwanted (coherent or decoherent) σ_z evolution generated by either $H_S(t)$ or $H_{SE}(t)$ or both, by subjecting the system to repeated spin flips. In group-theoretic terms such protocols have, as mentioned, a transparent interpretation as implementing an average over the group $\mathcal{Z}_2$, represented on $\mathcal{H}_S$ as $\hat{\mathcal{G}}=\{\hat{g}_\ell\}=\{\mathbb{1},\sigma_x\}$ [10]. The quantum operation effecting such group averaging is the projector $\Pi_{\mathcal{G}}$ on the space of operators commuting with $\hat{\mathcal{G}}$, leading to

$$\Pi_{\mathcal{G}}(\sigma_z) = \frac{1}{|\mathcal{G}|} \sum_{\hat{g}_\ell \in \mathcal{G}} \hat{g}_\ell^\dagger \sigma_z \hat{g}_\ell = \frac{1}{2}(\mathbb{1}\sigma_z\mathbb{1} + \sigma_x \sigma_z \sigma_x) = 0.$$

Essentially, in *cyclic* decoupling schemes based on $\mathcal{G}$ the above symmetrization is accomplished through a *time* average of the effective Hamiltonian determining the evolution over a cycle, T_c; in *random* schemes, it emerges from an *ensemble* average over different control histories, taken with respect to the uniform probability measure over $\mathcal{G}$ [36,42]. Neither deterministic nor stochastic sequences of π pulses achieve an exact implementation of $\Pi_{\mathcal{G}}$ for a fully generic Hamiltonian as in Eqs. (1) and (2), except in the ideal limit of arbitrarily fast control where the separation between pulses approaches zero. Therefore, it makes sense to compare the performance attainable by different control se-
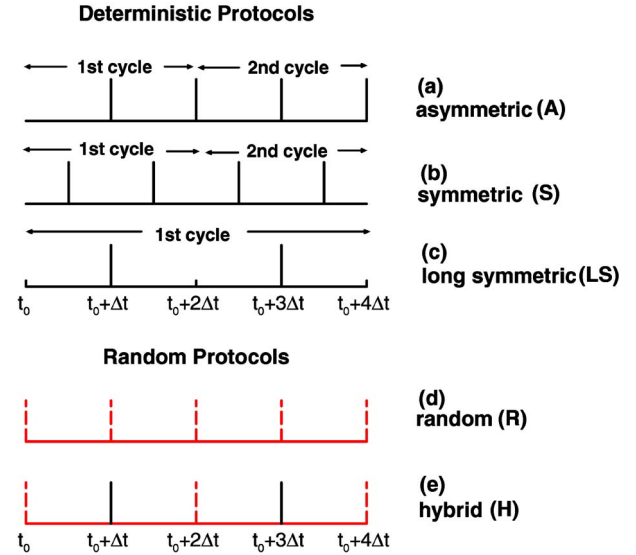

FIG. 1. (Color online) Pictorial representation of relevant control protocols used for coherence control. Deterministic pulses are indicated with solid vertical lines, while random pulses correspond to dashed vertical lines.

quences for realistic control rates. In this paper we shall focus on the following options.

(i) *Asymmetric cyclic protocol (A)*, Fig. 1(a). This is the protocol used in [9], corresponding to repeated spin echoes. Cyclicity is ensured by subjecting the system to an even number of equally spaced π pulses, applied at $t_j=t_0+j\Delta t$, $j=1,2,\ldots$, in the limit $\tau \to 0$. The elementary cycle consists of two pulses: the first one, applied after the system evolved freely for an interval Δt, reverses the qubit original state and the second one, applied a time Δt later, restores its original state.

(ii) *Symmetric cyclic protocol (S)*, Fig. 1(b). This protocol, which is directly inspired to the Carr-Purcell sequence of NMR, is obtained from (A) by rearranging the two π pulses within each cycle in such a way that the control propagator is symmetric with respect to the middle point. The first pulse is applied at $t_1=t_0+\Delta t/2$ and the next ones at $t_j=t_1+(j-1)\Delta t$, with $j>1$. Both the A and S protocols have a cycle time $T_c=2\Delta t$ and lead to the same averaging in the limit $\Delta t \to 0$. For finite Δt, however, the symmetry of the S protocol guarantees the cancellation of lowest-order corrections $\mathcal{O}(\Delta t)$, resulting in superior averaging [2,25,43].

(iii) *Long symmetric cyclic protocol (LS)*, Fig. 1(c). This is basically an S protocol with a doubled control interval $\Delta t \mapsto 2\Delta t$. Equivalently, note that this scheme corresponds to alternating a π pulse with the identity after every Δt. The cycle time becomes $T_c=4\Delta t$. For this amount of time, twice as many pulses would be used by protocols (A, S). Still, in certain cases, the LS protocol performs better than the A protocol (see Sec. V D), which motivates its separate consideration here.

(iv) *Naive random protocol (R)*, Fig. 1(d). Random decoupling is no longer cyclic, meaning that the control propagator does *not* necessarily effect a closed path (see also [20] for a discussion of acyclic deterministic schemes). The simplest random protocol in our setting corresponds to having, at each

time $t_j = t_0 + j\Delta t$, an equal probability of rotating or not the qubit; that is, at every t_j the control action has a 50% chance of being a π pulse and a 50% chance of being the identity. In order not to single out the first control slot, it is convenient to explicitly allow the value $j=0$ (equivalently, to consider a fictitious pulse $P_0 = \mathbb{1}$ in the A, S, and LS protocols). For pure phase errors as considered, such a protocol may be interpreted as a simplified PAREC scheme [38]. While we will mostly focus on this naive choice in our discussion here, several variants of this protocol may be interesting in principle, including unbalanced pulse probabilities and/or correlations between control operations.

(v) *Hybrid protocol (H)*, Fig. 1(e). Interesting control scenarios arise by combining deterministic and random design. The simplest option, which we call "hybrid" protocol here, consists of alternating, after every Δt, a π pulse with a random pulse, instead of the identity as in the LS protocol. For our system, in the embedded decoupling language of [39], this may be thought of as nesting the A and R protocols. In group-theoretic terms, the H protocol may be understood as *randomization over cycles* [36]. A complete asymmetric cycle may be constructed in two ways, say A_1 and A_2. Cycle A_1 corresponds to traversing $\mathcal{G}$ in the order $(\mathbb{1}, \sigma_x)$—that is, free evolution for Δt; first pulse; free evolution for Δt; second pulse—the cycle being completed right after the second pulse. Cycle A_2 corresponds to the reverse group path, $(\sigma_x, \mathbb{1})$. Thus, we have the following: pulse; free evolution for Δt; second pulse; and another free evolution for Δt—the system should be observed at this moment before any other pulse. The H protocol consists of uniformly picking at random one of the two cycles at every instant t_{2j}, where $j = 0, 1, \ldots$.

III. RANDOMIZED PHASE REFOCUSING IN AN ISOLATED QUBIT

A single qubit evolving according to unitary dynamics [$\mu=0$ in Eq. (2)] provides a pedagogical yet illustrative setting to study dynamical control. Since the goal here is to refocus the underlying phase evolution, the analysis of this system provides a transparent picture for the differences associated with deterministic and random pulses. It also simplifies the comprehension of the results for the more interesting case of a single qubit interacting with a decohering semiclassical or quantum environment, where the control purpose becomes twofold: phase refocusing and decoherence suppression.

A. Time-independent qubit Hamiltonian

We begin by considering the standard case of a time-independent target dynamics $\omega_0(t) \equiv \omega_0$ for all t. For all the control protocols illustrated above, the system evolves freely between pulses, with the propagator

$$U_0(t_{j+1}, t_j) = e^{-i\omega_0(t_{j+1}-t_j)\sigma_z/2}, \qquad (5)$$

whereas, during a pulse, it is only affected by the control Hamiltonian. The propagator for an instantaneous pulse applied at time $t=t_j$ will be indicated by P_j. Let

$$\rho(t) = \sum_{\ell,m=0,1} \rho_{\ell m}(t)|\ell\rangle\langle m| \qquad (6)$$

denote the qubit density operator in the computational basis $\{|0\rangle, |1\rangle\}$, with $\sigma_z|0\rangle = |0\rangle$ and $\sigma_z|1\rangle = -|1\rangle$. The relevant phase information is contained in the off-diagonal matrix element $\rho_{01}(t)$. If $\rho(t_0)$ is the initial qubit state, the time evolution after M control intervals under either deterministic or randomized protocols,

$$\rho(t_M) = U(t_M, t_0)\rho(t_0)U^\dagger(t_M, t_0), \qquad (7)$$

is dictated by a propagator of the form

$$
\begin{aligned}
U(t_M, t_0) &= \mathcal{T}\exp\left\{-i\int_{t_0}^{t_M}[H_0 + H_c(u)]du\right\} \\
&= P_M U_0(t_M, t_{M-1})P_{M-1}U_0(t_{M-1}, t_{M-2})\ldots P_1 U_0(t_1, t_0)P_0 \\
&= \underbrace{(P_M P_{M-1}\ldots P_1 P_0)}_{U_c(t_M)}(P_{M-1}\ldots P_1 P_0)^\dagger U_0(t_M, t_{M-1})(P_{M-1}\ldots P_1 P_0)\ldots U_0(t_2, t_1)(P_1 P_0)P_0^\dagger U_0(t_1, t_0)P_0,
\end{aligned}
$$

$$(8)$$

where $\mathcal{T}$ indicates, as usual, time ordering.

Recall the basic idea of deterministic phase refocusing. For the A protocol, $P_0 = \mathbb{1}$ and $P_j = \exp(-i\pi\sigma_x/2)$, $j \geq 1$ (see the Appendix). Exact averaging is then ensured after a single control cycle, thanks to the property

$$P_1^\dagger e^{-i\omega_0\Delta t\sigma_z/2}P_1 = e^{+i\omega_0\Delta t\sigma_z/2}. \qquad (9)$$

Thus, the total phase that the qubit would accumulate in the absence of control is fully compensated, provided that N complete cycles are effected (that is, an even number $M=2N$ of spin flips is applied). The overall evolution imple-

ments a stroboscopic no-op gate, $U(t_M, t_0) = \mathbb{1}$, $(t_M - t_0)$ $= M\Delta t = NT_c$, as desired [44]. Notice that the identity operator is also recovered with the S and LS protocols after their corresponding cycle is completed.

1. Control performance in the logical frame

In preparation to the randomized protocols (R,H), it is instructive to look at the system dynamics in a different frame. In particular, a formulation which is inspired by NMR [2] is the so-called *toggling-frame* or *logical-frame* picture, which corresponds to a time-dependent interaction representation with respect to the applied control Hamiltonian. Let

$$U_c(t,t_0) = \mathcal{T}\exp\left\{ -i \int_{t_0}^{t} H_c(u)du \right\} \quad (10)$$

denote the control propagator associated to $H_c(t)$. Then the transformed state is defined as

$$\tilde{\rho}(t) = U_c^\dagger(t,t_0)\rho(t)U_c(t,t_0), \quad (11)$$

with a tilde indicating henceforth logical-frame quantities. At the initial time t_0, the two frames coincide and $\tilde{\rho}(t_0) = \rho(t_0)$. The evolution operator in the logical frame is immediately obtained from Eqs. (7) and (11),

$$\tilde{U}(t,t_0) = U_c^\dagger(t,t_0)U(t,t_0), \quad (12)$$

with

$$\tilde{U}(t,t_0) = \mathcal{T}\exp\left\{ -i \int_{t_0}^{t} [U_c^\dagger(u)H_0 U_c(u)]du \right\}. \quad (13)$$

That is, the control field is *explicitly removed* from the effective logical Hamiltonian. Because, for BB multipulse control,

$$U_c(t_M, t_0) = P_M P_{M-1} \cdots P_1 P_0, \quad (14)$$

the expression for the logical frame propagator may simply be read off Eq. (8), yielding

$$\tilde{U}(t_M, t_0) = \mathcal{T}\left(\prod_{j=0}^{M-1} \mathcal{P}_j^\dagger U(t_{j+1}, t_j)\mathcal{P}_j \right), \quad (15)$$

in terms of the composite rotations

$$\mathcal{P}_j = P_j P_{j-1} \cdots P_1 P_0, \quad j = 0, \ldots, M-1.$$

For cyclic protocols, $U_c(t_M, t_0) = \exp(-iM\pi\sigma_x/2) = \mathbb{1}$ (M even); that is, the logical and physical frames overlap stroboscopically in time. Thus, $\tilde{U}(t_M, t_0) = \mathbb{1}$ and *phase refocusing in the logical frame is equivalent to phase refocusing in the physical frame*.

Now consider the evolution under the randomized protocols. The first pulse occurs at t_0, so after a time interval $t_M - t_0$ has elapsed, $M+1$ pulses have been applied. Since the final goal is to compare random with cyclic controls, we shall take M *even* henceforth. At time $t = t_M$, population inversion may have happened in general in the physical frame. This makes it both convenient and natural to consider the logical frame, where inversion does *not* happen, as the *pri-*

mary frame for control design. The evolution operator in this frame may be expressed, using Eq. (15), as

$$\tilde{U}(t_M, t_0) = \exp\left\{ -i\frac{\omega_0\Delta t}{2}\sigma_z \sum_{j=0}^{M-1} \chi_j \right\}, \quad (16)$$

where

$$\chi_j = (-1)^{\lambda_0 + \lambda_1 + \cdots + \lambda_j}, \quad j = 0, \ldots, M-1, \quad (17)$$

is a Bernoulli random variable which accounts for the history of spin flips up to t_j in a given realization. For each $m = 1, \ldots, j$, if a spin flip occurs at time t_m, then $\lambda_m = 1$ and $P_m = -i\sigma_x$; otherwise, $\lambda_m = 0$ and $P_m = \mathbb{1}$. Equivalently, χ_j will take the values $+1$ or -1 with equal probability, depending on whether the composite pulse $\mathcal{P}_j$ is the identity or a π pulse.

Let k be an index labeling different control realizations. For a fixed k, the qubit coherence in the logical frame is given by

$$\tilde{\rho}_{01}^{(k)}(t_M) = \exp\left(-i\omega_0\Delta t \sum_{j=0}^{M-1} \chi_j^{(k)} \right)\rho_{01}(t_0). \quad (18)$$

This expression provides the starting point for analyzing control performance. For the A protocol, the only possible realization has $\chi_j = (-1)^j$ and leads to the trivial result $\tilde{\rho}_{01}(t_M) = \rho_{01}(t_0)$. For the R protocol, realizations corresponding to different strings of λ's filling up M places give, in general, different phases and an ensemble average should be considered. If the statistical ensemble is large enough, the *average performance* may be approximated by the *expected performance*; which is obtained by averaging over *all* possible control realizations and will be denoted by $\mathbb{E}(\cdot)$. The calculation of the expectation value is straightforward in the *unbiased* setting considered here. Since, for each realization, $\chi_j = +1$ or -1 independently of the value of its predecessor χ_{j-1}, the following expression is found:

$$\mathbb{E}(\tilde{\rho}_{01}(t_M)) = \rho_{01}(t_0)[\cos(\omega_0\Delta t)]^M. \quad (19)$$

Several remarks are in order. Under random pulses, the phase accumulated during the interval $t_M - t_0 = M\Delta t$ is, on average, completely removed, regardless of the Δt value. An important distinction with respect to the deterministic controls, however, is that now the different phase factors carried by each stochastic evolution may interfere among themselves, causing the ensemble average to introduce an effective *phase damping*. In general, let us write the ensemble expectation in the form

$$\frac{\mathbb{E}(\tilde{\rho}_{01}(t_M))}{\rho_{01}(t_0)} = e^{i\phi_*(t_M, t_0)}e^{-\Gamma_*(t_M, t_0)}, \quad (20)$$

for real functions $\phi_*(t), \Gamma_*(t)$ [45]. Here, $\phi_*(t_M, t_0) = 0$, whereas $\Gamma_*(t_M, t_0) = -M \ln[\cos(\omega_0\Delta t)]$. Complete dephasing occurs when $\omega_0\Delta t = \ell'\pi/2$, with ℓ' odd, while for $\omega_0\Delta t = \ell\pi$, with $\ell \in \mathbb{Z}$, $\Gamma_*(t) = 0$. Whenever exact knowledge of the frequency ω_0 and precise control over the time interval Δt are available, the R protocol can be made to achieve exact averaging, like the A protocol, under the additional *synchronization condition* that

$$\Delta t = \ell \pi / \omega_0, \quad \ell \in \mathbb{Z}.$$

In situations where such a synchronization is not easily accessible, one may still look for a general condition under which the R protocol avoids ensemble dephasing. Taking a Taylor expansion of Eq. (19) yields

$$\omega_0^2 (t_M - t_0) \Delta t = \omega_0^2 (t_M - t_0)^2 / M \ll 1. \tag{21}$$

In principle, this requirement may be fulfilled by making t_M and/or Δt sufficiently small. Interestingly, the condition of Eq. (21) is directly related to the bound obtained in theorem 1 of [36] for the worst-case pure-state error probability, defined by

$$\varepsilon_t = \max_{|\psi\rangle} \{\varepsilon_t(|\psi\rangle)\} = 1 - \min_{|\psi\rangle} \mathbb{E}(\mathrm{Tr}[\rho(t_0)\tilde{\rho}(t)]), \tag{22}$$

where the latter term is the usual input-output state fidelity [4]. In the limit where $\|H_0(t)\|_2^2 \, t\Delta t \ll 1$, where $\|A\|_2 = \max|\mathrm{eig}(A)|, \ \forall A = A^\dagger$, theorem 1 implies

$$\varepsilon_t = \mathcal{O}(\|H_0(t)\|_2^2 \, t\Delta t). \tag{23}$$

On the other hand, using Eq. (19) we obtain

$$\varepsilon_{t_M}(|\psi\rangle) = 2\{\rho_{00}(t_0)\rho_{11}(t_0) - |\rho_{01}(t_0)|^2 [\cos(\omega_0 \Delta t)]^M\}.$$

For $\omega_0^2 (t_M - t_0) \Delta t \ll 1$, the above expression gives

$$\varepsilon_{t_M}(|\psi\rangle) \approx |\rho_{01}(t_0)|^2 \omega_0^2 (t_M - t_0) \Delta t, \tag{24}$$

$$\varepsilon_{t_M} = \mathcal{O}(\omega_0^2 (t_M - t_0) \Delta t), \tag{25}$$

which makes the connection with Eq. (21) manifest.

It remains to discuss the performance of the H protocol. The freedom of not always effecting a spin flip after every Δt, which is one of the appealing features of the R protocol, is still partially present here. On the other hand, since a spin flip does occur at every t_m with m odd, which leads to $\chi_j = -\chi_{j-1}$ for j odd, any realization of this protocol completely refocuses the qubit [see Eq. (18)], so $\phi_*(t_M, t_0) = 0$ and $\Gamma_*(t_M, t_0) = 0$. Accordingly, *in the logical frame, the H protocol is optimal*, combining the absence of phase damping of cyclic schemes with the flexibility of random pulses.

2. Ensemble averages: General remarks

In practice, we deal with the average performance of a statistical ensemble of size K. To evaluate the sample size that guarantees a desired margin of error δ [46], we invoke the central-limit theorem. Because different realizations are independent, the latter ensures that the average performance is distributed normally with a mean value equal to the expected performance and standard deviation given by $\sigma/\sqrt{K}$, where σ is the standard deviation for all realizations. Thus, if we want, with probability $(1-\epsilon)$, that the average performance differs from the expected performance by no more than δ, the sample size must be at least as large as

$$K_{\min} = \left(\frac{z_{\epsilon/2}\sigma}{\delta}\right)^2 = \mathcal{O}\left(\frac{\sigma^2}{\delta^2}\right), \tag{26}$$

where $z_{\epsilon/2}$ is the value of the standard normal variable which has a probability $\epsilon/2$ of being exceeded. Taking a Taylor

expansion of Eqs. (18) and (19), we can show that

$$\sigma = \mathcal{O}(\omega_0 \sqrt{(t_M - t_0)\Delta t}) \quad \text{for } \omega_0^2 (t_M - t_0)\Delta t \ll 1.$$

Thus, the number of realizations required to ensure a specified degree of precision decreases as Δt.

It is interesting to observe that the ensemble average may be interpreted as effecting a quantum operation

$$\mathbb{E}(\tilde{\rho}_{01}(t_M)) = \sum_k \frac{\tilde{U}^{(k)}}{\sqrt{2^M}} \tilde{\rho}(t_0) \frac{\tilde{U}^{(k)\dagger}}{\sqrt{2^M}},$$

with

$$\tilde{U}^{(k)}(t_M, t_0) = \alpha^{(k)} \mathbb{1} + \beta^{(k)} \sigma_z, \quad \sum_k \tilde{U}^{(k)\dagger} \tilde{U}^{(k)} = \mathbb{1},$$

and random coefficients $\alpha^{(k)}, \beta^{(k)}$ which may be derived from Eq. (16).

3. Control performances in the physical frame

Finally, it is important to compare the average coherence element in the logical and physical frames. Dephasing is a more delicate issue in the Schrödinger picture, because spin population is not necessarily conserved and $\rho_{01}(t_M)$ may be related to $\rho_{01}(t_0)$ or to $\rho_{10}(t_0)$, depending on how many π pulses occur. If, after an interval $t_M - t_0$, an even number of spin flips have happened, we recover $U_c(t_M, t_0) = \mathbb{1}$ as in the cyclic case, but an odd number of flips leads instead to $U_c(t_M, t_0) = \pm i\sigma_x$. By recalling Eq. (12), for randomized schemes we find

$$\mathbb{E}(\rho_{01}(t_M)) = \frac{\rho_{01}(t_0) + \rho_{10}(t_0)}{2} e^{-\Gamma_*(t_M, t_0)}, \tag{27}$$

where $\Gamma_*(t_M, t_0) = 0$ for the H protocol. Thus, the agreement between the expected results in the two frames depends on the initial qubit state. Results are identical if $\rho_{01}(t_0)$ is real, but differ otherwise. The worst scenario occurs if $\rho_{01}(t_0)$ is purely imaginary, as the average in the physical frame vanishes. This reflects the fact that the net evolution may be represented by a quantum operation that flips the state of the qubit with 50% probability and leaves it alone otherwise. Clearly, knowledge of the control history allows the system to be deterministically returned in the physical frame for any realization, if desired. That is, having a classical register that records the total number of spin flips may be used to select realizations that guarantee a good performance of random pulses also in the physical frame for any initial state. For example, if only realizations with an even number of spin flips are selected, the results in both frames are equal, $\mathbb{E}(\rho_{01}(t_M) \,|\, U_c(t_M, t_0 = \mathbb{1})) = \mathbb{E}(\tilde{\rho}_{01}(t_M))$, as desired.

To summarize, in the logical frame, refocusing the unwanted phase evolution is possible with any of the protocols we considered. The R protocol, however, introduces an average ensemble dephasing, which may only be prevented by precisely tuning $\Delta t = \ell \pi / \omega_0$, with $\ell \in \mathbb{Z}$, or by assuring that $\Delta t \ll 1/[\omega_0^2 (t_M - t_0)]$. This implies the appearance of a timescale requirement which is not present when dealing with deterministic controls or with the H protocol. In the physical

frame, state-independent conclusions regarding the system behavior may be drawn conditionally to specific subsets of control realizations. Overall, the H protocol emerges as an alternative of intermediate performance, which partially combines advantages from determinism and randomness.

B. Time-dependent qubit Hamiltonian

We now consider the more interesting case where the qubit frequency is time dependent, $\omega_0(t) = \omega_0 + \delta\omega_0(t)$, $\delta\omega_0(t) \equiv \omega_0 G(t)$ being a deterministic (but potentially unknown) function. This could result, for example, from uncontrolled drifts in the experimental apparatus.

While all protocols become essentially equivalent in the limit $M \to \infty$, searching for the best protocol becomes meaningful in practical situations where pulsing rates are necessarily finite. Under these conditions, the deterministic protocols described so far will no longer be able, in general, to completely refocus the qubit. This would require a very specific sequence of spin flips for each particular function $\delta\omega_0(t)$, which would be hard to construct under limited knowledge about the latter. On the other hand, the average over random realizations does remove the phase accumulated for *any* function $\delta\omega_0(t)$, making randomized protocols ideal choices for phase refocusing. As a drawback, however, ensemble dephasing may be introduced. Thus, the selection of a given protocol will be ultimately dictated by the resulting tradeoffs.

The propagator in the logical frame now reads

$$\tilde{U}(t_M, t_0) = \exp\left[-i\frac{\omega_0}{2}\sigma_z \sum_{j=0}^{M-1} \chi_j \int_{t_j}^{t_{j+1}} [1 + G(u)]du \right],$$
(28)

which reduces to Eq. (16) when $G(t) = 0$.

Some assumptions on both the amplitude and frequency behavior of $G(t)$ are needed in order to draw some general qualitative conclusions. First, if $|G(t)| \ll 1$, the analysis developed in the previous section will still approximately hold. In the spirit of regarding ω_0 as a central frequency, we will also discard the limit $|G(t)| \gg 1$ and restrict our analysis to cases where $\max_t |G(t)| \sim 1$. If $G(t)$ is dominated by frequency components which are very fast compared to $\tau_0 = \omega_0^{-1}$, the effect of $G(t)$ may effectively self-average out over a time interval of the order or longer than ω_0^{-1}. In the opposite limit, where the time dependence of $G(t)$ is significantly slower than ω_0, deterministic controls are expected to be most efficient in refocusing the qubit, improving steadily as Δt decreases. In intermediate situations, however, the deterministic performance may become unexpectedly poor for certain, in principle, unknown values of Δt. These features may be illustrated with a simple periodic dependence. Suppose, for example, that $G(t) = \sin(p\omega_0 t)$ and $p \in \mathbb{R}$. For a fixed time interval $t_f - t_0 < \pi/(p\omega_0)$, a significant reduction of the accumulated phase is already possible with few deterministic pulses. However, care must be taken to avoid unintended "resonances" between the natural and the induced sign change. For the A protocol, this effect is worst at Δt
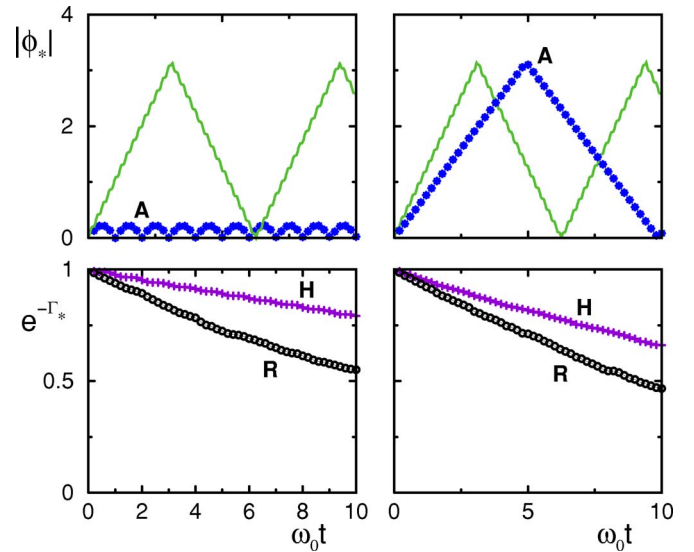

FIG. 2. (Color online) Accumulated phase (upper panels) and dephasing rate (lower panels) in the absence of control [solid (green) line], and under the A [(blue) stars], R [(black) circles], and H [(purple) plus] protocols in the logical frame, for $G(t) = \sin(p\omega_0 t)$ and $\Delta t = 1/(10\omega_0)$. Left panels: $p = 20\sqrt{2}$. Right panels: $p = 10\pi$. Average taken over 10^3 realizations. In this and all simulations that will follow, we set $t_0 = 0$.

$= \pi/(p\omega_0)$, in which case the control pulses exactly occur at the moment the function changes sign itself, hence precluding any cancellation of $G(t)$.

With the R protocol, ensemble dephasing becomes the downside to face. The ensemble average now becomes

$$e^{-\Gamma_*(t_M, t_0)} = \prod_{j=0}^{M-1} \cos\left\{ \omega_0 \left[\Delta t + \int_{t_j}^{t_{j+1}} G(u)du \right] \right\}. \quad (29)$$

In the absence of time dependence, phase damping is minimized as long as Eq. (21) holds. Under the above assumptions on $G(t)$, the condition remains essentially unchanged, in agreement with the fact that the accuracy of random averaging only depends on $\|H_0(t)\|_2$ [36].

Refocusing is also totally achieved with the H protocol. However, unlike in the case of the R protocol, the ensemble average no longer depends on the time-independent part of the Hamiltonian, but only on the function $G(t)$, making the identification of precise requirements on Δt harder in the absence of detailed information on the latter. We have

$$e^{-\Gamma_*(t_M, t_0)} = \prod_{j=0,2,4,\ldots}^{M-2} \cos\left\{ \omega_0 \left[\left(\int_{t_j}^{t_{j+1}} - \int_{t_{j+1}}^{t_{j+2}} \right) G(u)du \right] \right\}.$$
(30)

Figure 2 illustrates the points discussed so far. The sinusoidal example is considered, and we contrast the two aspects to be examined: the top panels show the phase magnitude $|\phi_*(t_M, t_0)|$, which is optimally eliminated with random pulses, while the bottom ones give the dephasing rate $e^{-\Gamma_*(t_M, t_0)}$, which is inexistent for deterministic controls. The interval between pulses is fixed, $\Delta t = 1/(10\omega_0)$, and the pro-
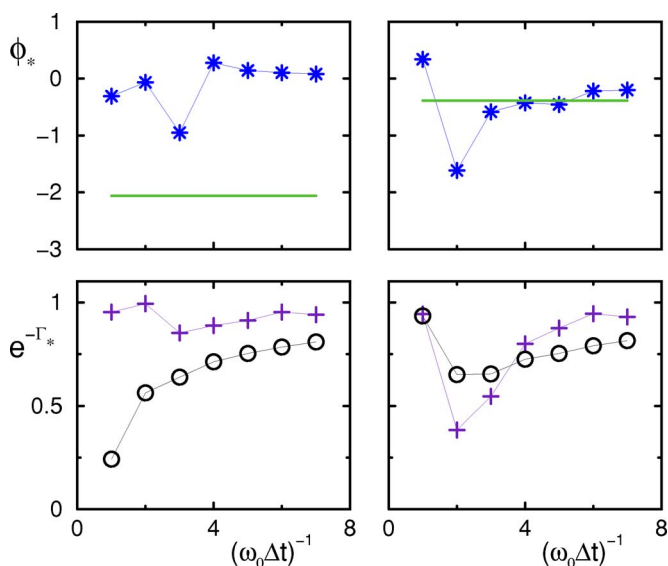
FIG. 3. (Color online) Accumulated phase (upper panels) and dephasing rate (lower panels) in the absence of control [solid (green) line] and under the A [(blue) stars], R [(black) circles], and H [(purple) plus] protocols in the logical frame. The time interval considered is $t_f=2/\omega_0$, and $(\omega_0\Delta t)^{-1}=M/2$ and $G(t)=\sin(p\omega_0 t)$, where $p=10$. The drift in the right panels includes $D(t) =(-1)^{\lfloor 10\omega_0 t/3\rfloor}$. Average taken over all possible realizations.

tocols are compared for two arbitrary, but relatively close values of the oscillation frequency rate: $p=20\sqrt{2}$ and $p=10\pi$. The deterministic control is very sensitive to slight changes of the drift and at certain instants may behave worse than if pulses were completely avoided. Similarly, the H protocol, even though more effective than the R protocol in this example, also suffers from uncertainties related to $G(t)$. On the contrary, deviations in the performance of the R protocol are practically unnoticeable, making it *more robust against variations in the system parameters*.

As a further illustrative example, we consider in Fig. 3 the following time dependence for the qubit:

$$\omega_0(t) = \omega_0[1 + G(t)]D(t). \tag{31}$$

The left panels have, as before, $D(t)=1$, while for the right panels,

$$D(t) = (-1)^{\lfloor 10\omega_0 t/3\rfloor}. \tag{32}$$

A fixed time $t_f=2/\omega_0$ is now divided into an increasing number M of intervals Δt. Here, selecting the most appropriate protocol depends on our priorities concerning refocusing and preservation of coherence. We may, however, as the right upper panel indicates, encounter *adversarial* situations where the time dependence of the qubit frequency is such that not acting on the system is comparatively better than using the A protocol. Clearly, depending on the underlying time dependence and the pulse separation, such poor performances are also expected to occur with other deterministic protocols. In addition, notice that, consistent with its hybrid nature, the H protocol may perform worse for values of Δt where the deterministic control becomes inefficient (compare right upper and lower panels). In similar situations, from the point of

view of its enhanced stability, *the R protocol turns out to be the method of choice*.

To summarize, an isolated qubit with time-dependent parameters provides the simplest setting where advantages of randomization begin to be apparent, in terms of enhanced stability against parameter variations. On average, phase is fully compensated, and ensemble dephasing may be kept very small for sufficiently fast control. Similar features will appear for a qubit interacting with a time-varying classical or quantum environment, as we shall see in Secs. IV C and V E.

IV. RANDOMIZED CONTROL OF DECOHERENCE FROM A SEMICLASSICAL ENVIRONMENT

Qubit coherence is limited by the unavoidable influence of noise sources. Within a semiclassical treatment, which provides an accurate description of decoherence dynamics whenever back-action effects from the system into the environment can be neglected, noise is modeled in terms of a classical stochastic process, effectively resulting in randomly time-dependent systems. Typically, external noise sources, which in a fully quantum description are well modeled by a *continuum* of harmonic modes (see Sec. V), are represented by a Gaussian process. Here, we focus on *localized* noise sources, which may be intrinsic to the physical device realizing the qubit—notably, localized traps or background charges, leading to a quantum *discrete* environment. In this case, non-Gaussian features become important and are more accurately represented in terms of noise resulting from a single or a collection of classical bistable fluctuators—leading to so-called random telegraph noise (RTN) or $1/f$ noise, respectively. Beside being widely encountered in a variety of different physical phenomena [47–49], such noise mechanisms play a dominant role in superconducting Josephson-junction-based implementations of quantum computers [50–53].

Recently, it has been shown that RTN and $1/f$ noise may be significantly reduced by applying cyclic sequences of BB pulses [22–26]. We now extend the analysis to randomized control. As it turns out, random decoupling is indeed viable and sometimes more stable than purely deterministic protocols. While a detailed analysis of randomized control of genuine $1/f$ noise would be interesting on its own, we begin here with the case of a single fluctuator. This provides an accurate approximation for mesoscopic devices where noise is dominated by a few fluctuators spatially close to the system [23,53–55]. Let the time-dependent Hamiltonian describing the noisy qubit be given by Eqs. (1) and (2), where $\mu=0$ and

$$\delta\omega_0(t) = \text{RNT}(t) \tag{33}$$

characterizes the stochastic process, randomly switching between two values $\pm v/2$, $v>0$. We shall in fact consider a *semirandom* telegraph noise; that is, we assume that the fluctuator initial state is always $+v/2$. The switching rate from $\pm v/2$ to $\mp v/2$ is denoted by $\gamma_{\mp}$, with $\gamma_+ + \gamma_- = \gamma$. We shall also assume for simplicity that $\gamma_+ = \gamma_-$, corresponding to a symmetrical process. The number of switching events $n(t,0)$ in a given time interval t is Poisson distributed as
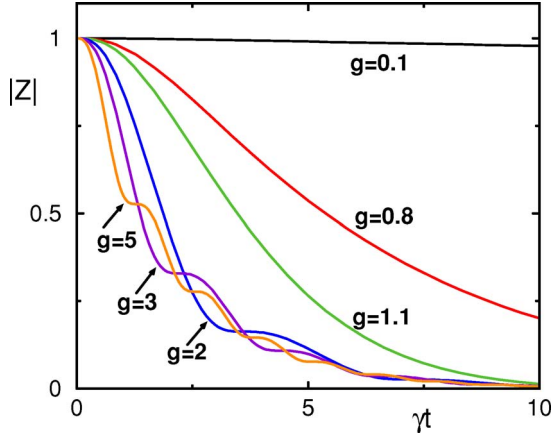
FIG. 4. (Color online). Decoherence rate $|Z(t)| = e^{-\Gamma(t)}$ from a symmetrical bistable fluctuator. Several values of $g = v/\gamma$ are considered, resulting from changing the coupling strength v at fixed switching rate $\gamma = 1$ a.u.

$$P\{n(t,0) = k\} = \frac{1}{k!}\left(\frac{\gamma t}{2}\right)^k e^{-\gamma t/2}.$$

Semiclassically, dephasing results from the ensemble average over different noise realizations. This leads to the decay of the average of the coherence element,

$$\frac{\langle \rho_{01}(t) \rangle}{\rho_{01}(t_0)} = e^{-i\omega_0(t-t_0)} Z(t,t_0),$$

$$Z(t,t_0) = e^{i\delta(t,t_0)} e^{-\Gamma(t,t_0)}. \tag{34}$$

Here, the average over RTN realizations is represented by $\langle \cdot \rangle$ and should be distinguished from the average over control realizations, which, as before, is denoted by $\mathbb{E}$. The dephasing factor $\Gamma(t,t_0)$ and the phase $\delta(t,t_0)$ have distinctive properties depending on the ratio $g = v/\gamma$, where $g < 1$ ($g > 1$) corresponds to a fast (slow) fluctuator. Given the initial condition for the fluctuator $\mathcal{E}_{p_0}$, where $\mathcal{E}_{p_0} = \pm 1$ stands for the fluctuator initially in state $\pm v/2$, $Z(t,t_0)$ may be calculated as [51]

$$Z(t,t_0) = C e^{-(\gamma/2)(1-\alpha)(t-t_0)} + (1-C)e^{-(\gamma/2)(1+\alpha)(t-t_0)}, \tag{35}$$

where

$$\alpha = \sqrt{1 - g^2 + 2ig\mathcal{E}_p}, \quad C = (1 + \alpha - ig\mathcal{E}_{p_0})/(2\alpha), \tag{36}$$

and $\mathcal{E}_p = (\gamma_- - \gamma_+)/\gamma$ is the equilibrium population difference. Note that for a symmetrical telegraph process, the only difference between the results for a fluctuator initially in state $+v/2$ or $-v/2$ is a sign in the above phase δ. The decoherence rate for a slow fluctuator is much more significant than for a fast fluctuator. This has been discussed in detail elsewhere [51] and has been reproduced for later comparison with the controlled case in Fig. 4, where several values of g are considered. A fast fluctuator behaves equivalently to an appropriate environment of harmonic oscillators, and noise effects are smaller for smaller values of g, whereas for a slow fluctuator the decoherence function saturates and becomes $\sim \gamma(t-t_0)$.

A. Deterministic and randomized controls in the interaction picture

Here we compare the reduction of RTN under the action of the A, H, and R protocols. In order to isolate the effects of the noise, it is convenient to first carry out the analysis in the interaction picture which removes the free dynamics $\omega_0\sigma_z/2$. The density operator becomes

$$\rho^I(t) = U^I(t,t_0)\rho(t_0)U^{I\dagger}(t,t_0), \tag{37}$$

where $U^I(t,t_0) = \exp(i\omega_0 t \sigma_z/2)$ and the superscript I will refer to the interaction picture henceforth. The free propagator between pulses is now

$$U^I(t_{j+1},t_j) = \mathcal{T}\exp\left\{-i\int_{t_j}^{t_{j+1}} H_0^I(u)du\right\}, \tag{38}$$

with $H_0^I(t) = \delta\omega_0(t)\sigma_z/2$, while at t_j, we have (see the Appendix)

$$P_j^I = \exp\left[i\frac{\omega_0 t_j}{2}\sigma_z\right]\exp\left[-i\lambda_j\frac{\pi}{2}\sigma_x\right]\exp\left[-i\frac{\omega_0 t_j}{2}\sigma_z\right]. \tag{39}$$

A second canonical transformation into the logical frame is also considered, so that (as before) realizations with an even or an odd number of total spin flips are treated on an equal footing. We will refer to the combination of the two transformations as the logical-IP frame. Similarly to Eq. (12), the interaction and the logical-IP frame propagators are related as

$$\tilde{U}^I(t,t_0) = U_c^{\dagger I}(t,t_0)U^I(t,t_0). \tag{40}$$

This leads to the following propagators at t_M:

$$U_c^I(t_M,t_0) = \mathcal{T}\left(\prod_{j=0}^M P_j^I\right),$$

$$\tilde{U}^I(t_M,t_0) = \mathcal{T}\left(\prod_{j=0}^{M-1}\mathcal{P}_j^{\dagger I}U^I(t_{j+1},t_j)\mathcal{P}_j^I\right),$$

where

$$\mathcal{P}_j^I = P_j^I P_{j-1}^I \cdots P_2^I P_1^I P_0^I, \quad j = 0,\dots,M-1.$$

Our goal is to compute the ratio

$$F(t_M,t_0) = \frac{\mathbb{E}(\langle\tilde{\rho}_{01}^I(t_M)\rangle)}{\rho_{01}(t_0)} \approx \frac{\langle\mathbb{E}(\tilde{\rho}_{01}^I(t_M))\rangle}{\rho_{01}(t_0)}$$

$$= \mathbb{E}(e^{i\delta^{(k)}(t_M,t_0)}e^{-\Gamma^{(k)}(t_M,t_0)}), \tag{41}$$

where k labels, as before, different control realizations. Note that interchanging the order of the averages does *not* modify the results if all pulse realizations are considered and the number of RTN realizations is large enough. With 10^5 switch realizations no significant variations were found by interchanging the averages.

The decoherence rate $|F(t_M,t_0)|$ for the three selected protocols is shown in Fig. 5, where a time $t_f = 10/\gamma$ was fixed and divided into an increasing number M of intervals Δt. The left panels are obtained for three slow fluctuators, $g = 5, 3, 2$, and the right panels for $g = 1.1, 0.8, 0.1$. These are the six
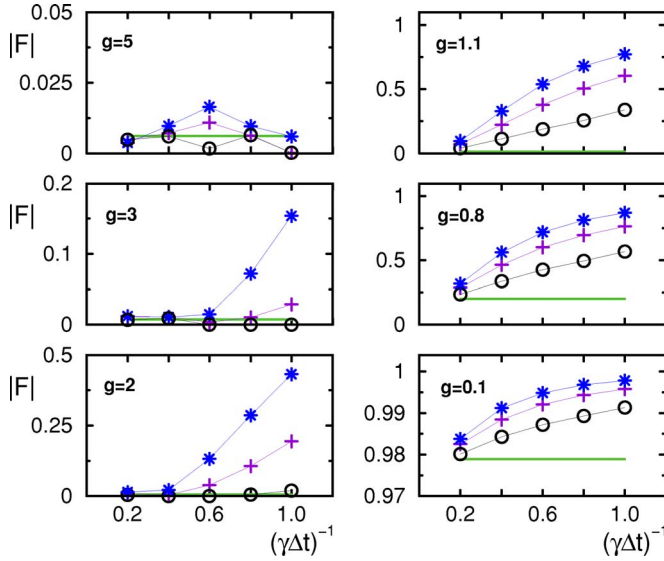
FIG. 5. (Color online) Decoherence rate from a symmetrical bistable fluctuator with $g=5,3,2,1.1,0.8,0.1$. (Green) solid lines represent the analytical results from [51] in the absence of control. (Blue) stars: A protocol. (Black) circles: R protocol (Purple) plus: H protocol. Averages are taken over 10^5 RTN realizations and all possible 2^M pulse realizations. The time interval considered is $t_f=10/\gamma$, thus $(\gamma\Delta t)^{-1}=M/10$.

different noise regimes considered in Ref. [24], where the A protocol was studied. The authors concluded that once $\Delta t \ll 1/\gamma$, $\Gamma(t_M,t_0)$ scales with g^2, while for $\Delta t \gtrsim 1/\gamma$, BB pulses are still capable of partially reducing noise due to a fast fluctuator, but are mostly inefficient against slow fluctuators. Here, we verified that among all possible realizations of pulses separated by the same interval Δt, the realization corresponding to the A protocol yields the largest value of $|F(t_M,t_0)|$, whereas the absence of pulses gives, as expected, the smallest value. This justifies why, in terms of average performance for finite Δt, we have, in decreasing order, A, H, and R protocols, while for $M \to \infty$, different protocols are expected to become equivalent.

In terms of refocusing the unwanted phase evolution, the above-randomized protocols are optimal, since $\mathrm{Arg}(\langle \mathbb{E}(\tilde{\rho}^I_{01}(t_M)) \rangle / \rho_{01}(t_0))=0$, while the phase magnitude $\delta(t_M,t_0)$ for the A protocol is eventually compensated as M increases. This is shown in Fig. 6. Notice also that the absolute phase is very small for fast fluctuators.

Instead of fixing a time t_f, an alternative picture of the performance of different protocols may also be obtained by fixing the number of intervals M, as in Fig. 7 (left panels). As expected, a larger M leads to coherence preservation for longer times. Still another option is to fix the interval between pulses Δt, as in Fig. 7 (right panel). As before, the A protocol shows the best performance, followed by the H and R protocols.

B. Randomized control in the physical frame

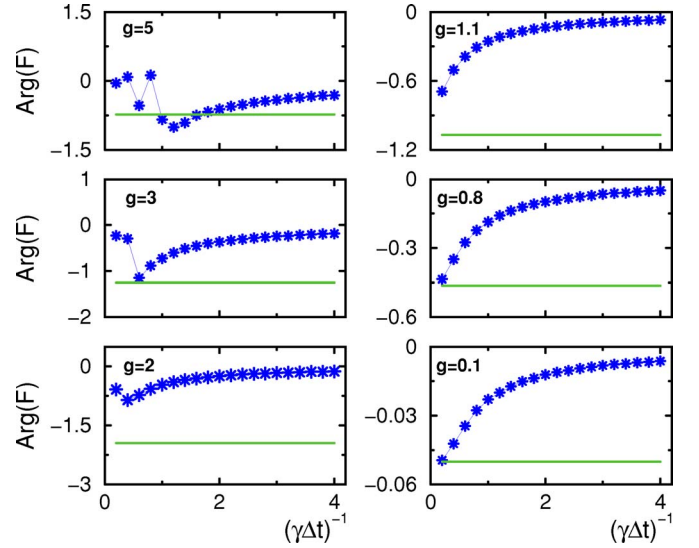If the interaction picture is not taken into account, complete refocusing is again guaranteed, on average, when either the R or H protocol is used. However, for the R protocol, the qubit frequency plays a delicate role in the resulting dephasing process. We now have

$$\mathbb{E}(\langle \tilde{\rho}_{01}(t_M) \rangle) = \rho_{01}(t_0)$$
$$\times \mathbb{E}\left(\exp\left(-i\omega_0\Delta t \sum_{j=0}^{M-1} \chi_j^{(k)} + i\delta^{(k)}(t_M,t_0) \right) e^{-\Gamma^{(k)}(t_M,t_0)} \right), \qquad (42)$$

which may be further simplified as follows. Among the 2^M

FIG. 6. (Color online) Phase offset from a symmetrical bistable fluctuator with $g=5,3,2,1.1,0.8,0.1$. (Green) solid line: analytical results in the absence of control pulses. (Blue) stars: A protocol; both R and H protocols have phase equal to zero. The time interval considered is $t_f=10/\gamma$, so $(\gamma\Delta t)^{-1}=M/10$. Averages computed as in Fig. 5.
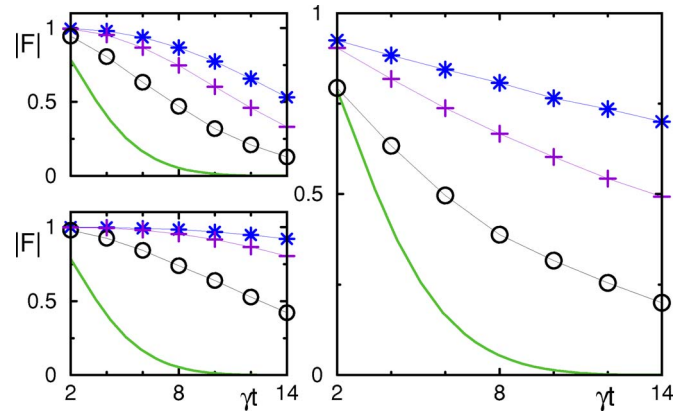

FIG. 7. (Color online) Decoherence rate from a symmetrical bistable fluctuator with $g=1.1$. Left panels: $M=10$ (top), $M=30$ (bottom). Right panel: $\Delta t=1/\gamma$. (Green) solid line: analytical results in the absence of control. (Blue) stars: A protocol. (Black) circles: R protocol. (Purple) plus: H protocol. Averages are taken over 10^4 RTN realizations and 10^3 pulse realizations.

pulse realizations existing in the logical frame, there are pairs, say, corresponding to labels k and k', where $\lambda_0^{(k)}=1$ and $\lambda_0^{(k')}=0$, while $\lambda_j^{(k)}=\lambda_j^{(k')}$ with $1 \leqslant j \leqslant M-1$, which leads to $\sum_{j=1}^{M-1}\chi_j^{(k)}=-\sum_{j=1}^{M-1}\chi_j^{(k')}$. Besides, since we are considering a semirandom telegraph noise, a pulse at t_0 is equivalent to switching the fluctuator from the initial state $+v/2$ to $-v/2$, whose net effect is simply a change in the sign of the phase $\delta(t_M,t_0)$. Therefore, we may write

$$\mathbb{E}(\langle \widetilde{\rho}_{01}(t_M)\rangle) = \frac{\rho_{01}(t_0)}{2^{M-1}} \sum_{k=1}^{2^{M-1}} \{\cos[\Xi_{M-1}^{(k)}\omega_0\Delta t$$
$$- \delta^{(k)}(t_M,t_0)]e^{-\Gamma^{(k)}(t_M,t_0)}\}, \qquad (43)$$

where

$$\Xi_{M-1}^{(k)} = 1 + \sum_{j=1}^{M-1} \chi_j^{(k,1)}, \quad M \geqslant 2, \qquad (44)$$

and $\chi_j^{(k,1)}=(-1)^{\lambda_1^{(k)}+\lambda_2^{(k)}+\cdots+\lambda_j^{(k)}}$.

In the physical frame, we find, correspondingly,

$$\mathbb{E}(\langle \rho_{01}(t_M)\rangle) = \frac{\rho_{01}(t_0)+\rho_{10}(t_0)}{2^M} \sum_{k=1}^{2^{M-1}} \{\cos[\Xi_M^{(k)}\omega_0\Delta t$$
$$- \delta^{(k)}(t_M,t_0)]e^{-\Gamma^{(k)}(t_M,t_0)}\}. \qquad (45)$$

Contrary to the result obtained in the absence of noise, Eq. (19), the additional realization-dependent phase shift $\delta^{(k)}(t_M,t_0)$ now remains. While, on average, this phase is removed in the limit where $\Delta t \to 0$, for finite control rates $\delta^{(k)}(t_M,t_0)$ may destructively interfere with the phase gained from the free evolution, potentially increasing the coherence loss. Identifying specific values of Δt where such harmful interferences may happen for the given RTN process is not possible, which makes the results for the R protocol with finite Δt unpredictable in this case.

While the above feature is a clear disadvantage, it is avoided by the H protocol. For each realization, the phase accumulated with the free evolution is completely canceled, so the result in the logical-IP frame is equal to that in the logical frame: $\mathbb{E}(\langle \widetilde{\rho}_{01}(t_M)\rangle)=\mathbb{E}(\langle \widetilde{\rho}_{01}^I(t_M)\rangle)$. If access to a classical register that records the total number of spin flips is also available, this equivalence between frames may be further extended to the physical frame. Additionally, as already found in Sec. III B, randomized protocols tend to offer superior stability.

C. Deterministic bursts of switches

Let us illustrate the above statement through an example where the noisy dynamics of the system is slightly perturbed. Suppose that, moving back to the interaction picture, the noise process is now

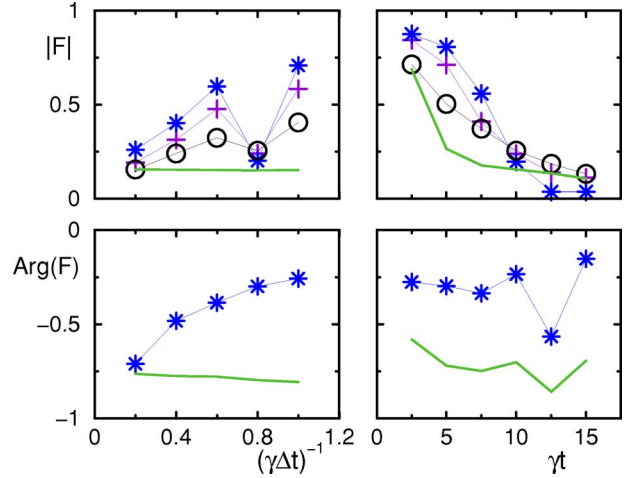$$H^I = D(t)\frac{\text{RNT}(t)}{2}\sigma_z, \qquad (46)$$

where

FIG. 8. (Color online) Decoherence rate (upper panels) and phase offset (lower panels) in the logical-IP frame for a single fluctuator with $g=1.1$ subjected to a disturbance as given in Eq. (47). Left panels: fixed $t_f=10/\gamma$, so $(\gamma\Delta t)^{-1}=M/10$. Right panels: fixed $\Delta t=5/(4\gamma)$. (Green) solid line: results in the absence of control pulses. (Blue) stars: A protocol. (Black) circles: R protocol. (Purple) plus: H protocol. The average phase for both R and H protocols is zero. Left panels: averages are taken over 10^5 RTN realizations and all possible 2^M pulse realizations. Right panels: averages are taken over 10^4 RTN realizations and 10^3 pulse realizations.

$$D(t) = (-1)^{\lfloor 4\gamma t/25\rfloor \lfloor 4\gamma t/5\rfloor}. \qquad (47)$$

Physically, $D(t)$ describes a sequence of six instantaneous switches, equally separated by the interval $5/(4\gamma)$, restarting again at every instant $25k/(4\gamma)$, k being an odd number. This process may be viewed as bursts of switches of duration $25/(4\gamma)$ followed by an interval $25/(4\gamma)$ of dormancy. The resulting behavior for $g=1.1$ in the logical-IP frame is depicted in Fig. 8.

With deterministic control, the rate of noise suppression quickly improves as the separation between pulses shrinks (left upper panel), until a certain value $\Delta t=t_f/8=5/(4\gamma)$, where it suddenly shows a significant recoil, becoming almost as bad as simply not acting on the system at all. Equivalently, by fixing $\Delta t=5/(4\gamma)$, the performance of the A protocol becomes very poor for $t \geqslant 10/\gamma$ (right upper panel). In practice, detailed knowledge of the system dynamics might be unavailable, making it impossible to predict which values of Δt might be adverse. Randomized schemes, on the other hand, are by their own nature more stable against such interferences. As seen from the figure, the R protocol shows a slower, but also more consistent improvement as Δt decreases and might therefore be safer in such conditions. Notice also that, in terms of coherence preservation and stability, the H protocol shows (as intuitively expected) an intermediate performance between the A and R protocols.

To summarize, in the logical-IP frame, the effects of the RTN can be reduced not only under deterministic pulses, but also with a randomized control, though a comparatively shorter pulse separation is needed in the latter case. In the logical and physical frames, the R protocol, besides showing the poorest performance among the three considered

schemes, may also lead to dangerous interferences between the qubit frequency and the phase gained from the free evolution. Such a problem, however, does not exist for the H protocol. The benefits of randomization are most clear when limited knowledge about the system dynamics is available and deterministic control sequences may be inefficient in avoiding unwanted "resonances." Combining protocols, where we gain stability from randomness, but also avoid the free phase evolution, is desirable especially when working in the physical frame. In this sense, the H protocol emerges as a promising compromise.

V. RANDOMIZED CONTROL OF DECOHERENCE FROM A QUANTUM BOSONIC ENVIRONMENT

We now analyze the case of a genuine quantum reservoir, where decoherence arises from the entanglement between the qubit and environment. The relevant Hamiltonian is given by Eqs. (1) and (2) with $\omega_0(t) = \omega_0$ and $\mu = 1$. In the semiclassical limit, the effects of the interaction with the bosonic degrees of freedom may be interpreted in terms of an external noise source whose fluctuations correspond to a Gaussian random process.

A detailed analysis of deterministic decoherence suppression for this model was carried out in [9] (see also [56] for an early treatment of the driven spin-boson model in a nonresonant monochromatic field and [57] for related discussions of dynamically modified relaxation rates). Here, we discuss how randomized decoupling performs.

A. Free solution for time-independent interaction Hamiltonian

As in Sec. IV, we first focus on understanding the controlled dynamics in a frame that explicitly removes both the control field and the free evolution due to $H_S \otimes 1 + 1 \otimes H_E$. Let us recall some known results related to the uncontrolled dynamics. We have [9,40]

$$U^I(t, t_0) = \exp\left\{\frac{\sigma_z}{2} \otimes \sum_k [b_k^\dagger e^{i\omega_k t_0} \xi_k(t - t_0) - \text{H.c.}]\right\},$$

(48)

where

$$\xi_k(\Delta t) = \frac{2g_k}{\omega_k}(1 - e^{i\omega_k \Delta t}).$$

(49)

Under the standard assumptions that the qubit and environment are initially uncorrelated,

$$\rho_{\text{tot}}(t_0) = \rho(t_0) \otimes \rho_E(t_0),$$

and that the environment is in thermal equilibrium at temperature T (the Boltzmann constant is set $= 1$),

$$\rho_E(t_0) = \prod_k \rho_{E,k}(T) = \prod_k (1 - e^{\omega_k/T})e^{-\omega_k b_k^\dagger b_k/T},$$

the trace over the environment degrees of freedom may be performed analytically, leading to the following expression for the qubit coherence:

$$\rho_{01}^I(t) = \rho_{01}(t_0)\prod_k \text{Tr}_k\{\rho_{E,k}(T)\mathcal{D}[e^{i\omega_k t_0}\xi_k(t - t_0)]\}$$

$$= \rho_{01}(t_0)\exp[-\Gamma(t, t_0)].$$

(50)

Here, $\mathcal{D}(\xi_k) = \exp(b_k^\dagger \xi_k - b_k \xi_k^*)$ is the harmonic displacement operator of the kth bath mode and the decoherence function $\Gamma(t, t_0)$ is explicitly given by

$$\Gamma(t, t_0) = \sum_k \frac{|\xi_k(t - t_0)|^2}{2}\coth\left(\frac{\omega_k}{2T}\right).$$

(51)

In the continuum limit, substituting $\Sigma_k \delta(\omega - \omega_k)|g_k|^2$ by the spectral density $I(\omega)$, one finds

$$\Gamma(t, t_0) = 4\int_0^\infty d\omega I(\omega)\coth\left(\frac{\omega}{2T}\right)\frac{1 - \cos[\omega(t - t_0)]}{\omega^2}.$$

(52)

For frequencies less than an ultraviolet cutoff ω_c, $I(\omega)$ may be assumed to have a power-law behavior,

$$I(\omega) = \frac{\alpha}{4}\omega^s e^{-\omega/\omega_c}.$$

(53)

The parameter $\alpha > 0$ quantifies the overall system-bath interaction strength, and s classifies different environment behaviors: $s = 1$ corresponds to the Ohmic case, $s > 1$ to the super-Ohmic, and $0 < s < 1$ to the sub-Ohmic case.

B. Randomly controlled decoherence dynamics: Analytical solution and error bound

Remarkably, the dynamics remains exactly solvable in the presence of randomized BB kicks. We focus first on the R protocol viewed in the logical-IP frame. Between pulses the evolution is characterized by Eq. (48), while at t_j Eq. (39) applies. Using Eq. (40), the propagator in the logical-IP frame, apart from an irrelevant overall phase factor, may be finally written as

$$\tilde{U}^I(t_M, t_0) = \exp\left\{\frac{\sigma_z}{2} \otimes \sum_k [b_k^\dagger e^{i\omega_k t_0}\eta_k^R(M, \Delta t) - \text{H.c.}]\right\},$$

(54)

where

$$\eta_k^R(M, \Delta t) = \sum_{j=0}^{M-1}\chi_j e^{i\omega_k j\Delta t}\xi_k(\Delta t).$$

(55)

Under the uncorrelated initial conditions specified above and thermal equilibrium conditions, the qubit reduced density matrix is exactly computed as

$$\tilde{\rho}_{01}^I(t_M) = \rho_{01}(t_0)\prod_k \text{Tr}_k\{\rho_{E,k}(T)\mathcal{D}[e^{i\omega_k t_0}\eta_k^R(M, \Delta t)]\}$$

$$= \rho_{01}(t_0)e^{-\Gamma_R(t_M, t_0)}.$$

(56)

Because χ_j in Eq. (55) can be ± 1 at random, each element in the sum corresponds to a vector in the complex plane with a different orientation at every step Δt. Thus, the displacement

operator above may be suggestively interpreted as a random walk in the complex plane.

The decoherence function $\Gamma_R(t_M, t_0)$ is now given by

$$\Gamma_R(t_M, t_0) = \sum_k \frac{|\eta_k^R(M, \Delta t)|^2}{2} \coth\left(\frac{\omega_k}{2T}\right), \qquad (57)$$

which, in the continuum limit, becomes

$$\Gamma_R(t_M, t_0) = 4 \int_0^\infty d\omega I(\omega) \coth\left(\frac{\omega}{2T}\right) \frac{1 - \cos(\omega \Delta t)}{\omega^2}$$
$$\times \left[M + 2 \sum_{j=1}^{M-1} \cos(j\omega\Delta t) \sum_{\ell=0}^{M-j-1} \chi_\ell \chi_{\ell+j} \right].$$
$$(58)$$

The decoherence behavior under the A protocol is obtained by letting $\chi_j = (-1)^j$. We then recover the result of deterministically controlled decoherence [9], which may be further simplified as [22,43]

$$\Gamma_D(t_M, t_0) = 4 \int_0^\infty d\omega I(\omega) \coth\left(\frac{\omega}{2T}\right)$$
$$\times \frac{1 - \cos[\omega(t_M - t_0)]}{\omega^2} \tan^2\left(\frac{\omega \Delta t}{2}\right). \quad (59)$$

Before proceeding with a numerical comparison between Eqs. (58) and (59), some insight may be gained from an analytical lower bound for the average $\mathbb{E}(\exp[-\Gamma_R(t_M, t_0)])$. According to Jensen's inequality, $\mathbb{E}(f(x)) \geqslant f(\mathbb{E}(x))$ for any convex function f. Using this and the fact that

$$\mathbb{E}(\chi_\ell \chi_{\ell+j}) = \mathbb{E}((-1)^{\lambda_{\ell+1} + \lambda_{\ell+2} + \cdots + \lambda_{\ell+j}}) = 0,$$

we have the lower bound

$$\mathbb{E}(\exp[-\Gamma_R(t_M, t_0)]) \geqslant \exp[-\mathbb{E}(\Gamma_R(t_M, t_0))],$$

$$\mathbb{E}(\Gamma_R(t_M, t_0)) = 4M \int_0^\infty d\omega I(\omega) \coth\left(\frac{\omega}{2T}\right) \frac{1 - \cos(\omega \Delta t)}{\omega^2}.$$
$$(60)$$

In Fig. 9 we compare the coherence decay corresponding to the absence of control (52), to the A protocol (59) and to the lower bound (60). Two limiting cases of high and low temperature, $T \gg \omega_c$ and $T \ll \omega_c$, are considered. The high-temperature limit corresponds to an effectively classical bath, where the properties of the environment are dominated by thermal fluctuations. In the absence of control, decoherence is very fast on the time scale determined by the bath correlation time $\tau_c = \omega_c^{-1}$; hence, coherence preservation requires very short intervals between pulses. The A protocol shows the best performance. The actual randomized performance may, however, be significantly better than the lower bound in this temperature regime, though they never surpass the deterministic case (see next subsection).

In the case of low temperature, or a fully quantum bath, decoherence is much slower and a richer interplay between thermal and vacuum fluctuations occurs. Larger values of Δt may then be analyzed before total coherence loss takes place.
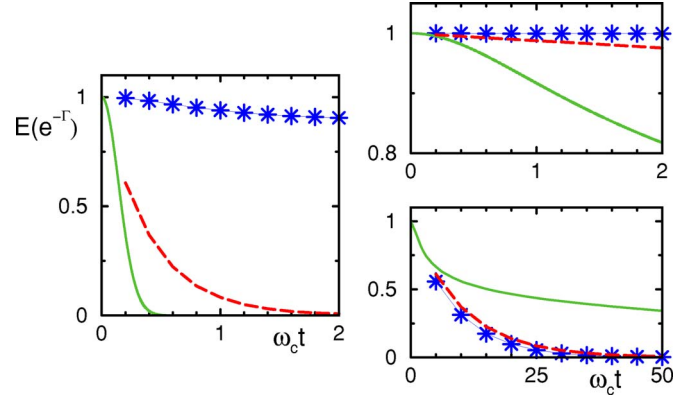

FIG. 9. (Color online) Decoherence rate from a bosonic Ohmic bath. Here and in the following figures, time is measured in units of T^{-1}, $\alpha = 0.25$, and $\omega_c = 100$. Left panel: $T = 10^2 \omega_c$ and $\omega_c \Delta t = 0.1$. Right panels: $T = 10^{-2} \omega_c$. Top: $\omega_c \Delta t = 0.1$. Bottom: $\omega_c \Delta t = 2.5$. (Green) solid line: no control. (Blue) stars: A protocol. (Red) dashed line: lower bound, Eq. (60).

The interesting phenomenon of decoherence acceleration [9,58], which may happen when $\omega_c \Delta t > 1$, may now be observed. For short Δt, the A protocol is again more efficient, though not significantly better than the lower bound. For large Δt, pulses induce destructive interference and the A protocol performs even worse than the lower bound. In such situation the best option is simply not to act on the system.

When $\omega_c \Delta t \lesssim 1$, some general insight may be gained by comparing appropriate limits of the lower bound and the deterministic decoherence function. First, by Taylor expanding up to second order in Δt we have

$$\mathbb{E}(\Gamma_R(t_M, t_0)) \approx 2(t_M - t_0)\Delta t \int_0^\infty d\omega I(\omega) \coth\left(\frac{\omega}{2T}\right), \quad (61)$$

whereas

$$\Gamma_D(t_M, t_0) \approx \Delta t^2 \int_0^\infty d\omega I(\omega) \coth\left(\frac{\omega}{2T}\right) \{1 - \cos[\omega(t_M - t_0)]\}.$$
$$(62)$$

Therefore, in the limit of very short Δt, the lower bound approaches the ideal situation of total suppression of decoherence linearly in Δt, while for the A protocol this occurs quadratically.

This analysis may be further extended by studying the two limits of Eq. (61) with respect to temperature. Considering the spectral density of Eq. (53), we have

$$T \gg \omega_c: \quad \mathbb{E}(\Gamma_R(t_M, t_0)) = \mathcal{O}(\alpha T \omega_c^s (t_M - t_0)\Delta t),$$

$$T \ll \omega_c: \quad \mathbb{E}(\Gamma_R(t_M, t_0)) = \mathcal{O}(\alpha \omega_c^{s+1} (t_M - t_0)\Delta t).$$

Thus, a sufficient condition under which random control avoids decoherence is

$$T \gg \omega_c: \quad \alpha T \omega_c^s (t_M - t_0)\Delta t \ll 1,$$

$$T \ll \omega_c: \quad \alpha \omega_c^{s+1}(t_M - t_0)\Delta t \ll 1.$$

This should be compared with the general bound given in theorem 2 of [36]. We will see in Sec. V D that, in the physical frame, the qubit frequency ω_0 also plays an important role.

A similar analysis for the A protocol may be effected using Eq. (62). For $\omega_c(t_M - t_0) \ll 1$, the decoherence function decays quadratically in time, giving

$$T \gg \omega_c: \quad \Gamma_D(t_M, t_0) = \mathcal{O}(\alpha T \omega_c^{s+2}(t_M - t_0)^2 \Delta t^2),$$

$$T \ll \omega_c: \quad \Gamma_D(t_M, t_0) = \mathcal{O}(\alpha \omega_c^{s+3}(t_M - t_0)^2 \Delta t^2),$$

while for $\omega_c(t_M - t_0) \gg 1$ the decoherence function becomes independent of $t_M - t_0$, and we get

$$T \gg \omega_c: \quad \Gamma_D(t_M, t_0) = \mathcal{O}(\alpha T \omega_c^s \Delta t^2),$$

$$T \ll \omega_c: \quad \Gamma_D(t_M, t_0) = \mathcal{O}(\alpha \omega_c^{s+1} \Delta t^2).$$

These should be compared with the error bound of theorem 3 in [36]. Based on these considerations, random pulses may hardly be expected to outperform deterministic controls in the limits discussed above. Still, it remains interesting to quantitatively see what the actual performance is for intermediate Δt and/or hybrid schemes—for instance, with respect to acceleration. Moreover, further changes may be expected when some time dependence exists in the system parameters—for instance, in the coupling strength to the environment (see Sec. V E).

C. Randomly controlled decoherence dynamics: Numerical results

Based on the exact result of Eq. (58), we now present a comparison of the average decoherence suppression achievable by the protocols described in Sec. II. A fixed time t_f divided into an increasing number M of intervals Δt is considered.

Figure 10 compares the average $\mathbb{E}(\exp[-\Gamma_R(t_M, t_0)])$ in the limit of high temperature, $T = 10^2 \omega_c$, for a system evolving under the A and R protocols. For the fixed times chosen, $\omega_c t_f = 0.5$ (upper panel) and $\omega_c t_f = 1$ (lower panel), the coherence element has already practically disappeared and cannot be seen in the figure, while the A protocol is able to recover it even for very few cycles. The values of $\exp[-\Gamma_R(t_M, t_0)]$ for different realizations are widely spread between the worst case corresponding to all $\lambda = 0$ and the efficient realizations involving several spin flips. As a consequence, the average converges to 1 slowly and has a large standard deviation [59]. Notice, however, that it is significantly better than the lower bound.

The results in the low-temperature limit, $T = 10^{-2} \omega_c$, are shown in Fig. 11. Here, thanks to the fact that decoherence is overall slower, longer evolution times may be chosen: $\omega_c t_f = 1$ (upper panel) and $\omega_c t_f = 10$ (lower panel). For the latter choice, in particular, when $M \lesssim 10$, decoherence enhancement occurs and, interestingly, the results for the A protocol are *worse* than those for the R protocol. However, it
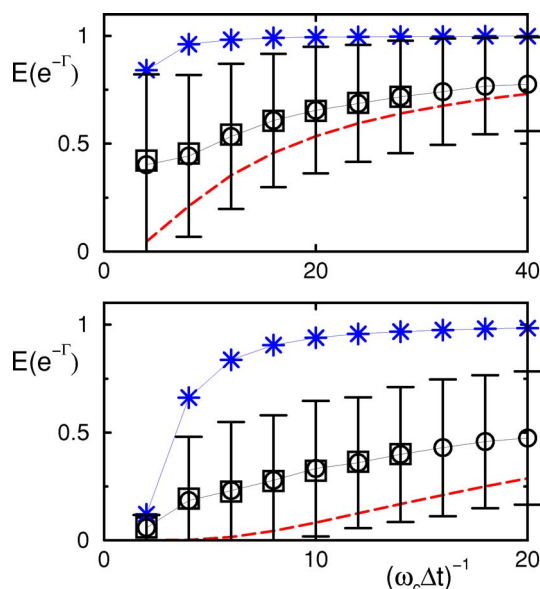

FIG. 10. (Color online) Decoherence rate for a high-temperature Ohmic bath, $T = 10^2 \omega_c$. Upper panel: $\omega_c t_f = 0.5$. Lower panel: $\omega_c t_f = 1$. (Blue) stars: A protocol. (Black) circles: average over 10^3 realizations and respective standard deviations for the R protocol [59]. (Black) squares: expectation value (taken over all 2^M realizations) for the R protocol. (Red) dashed line: lower bound.

takes a much smaller Δt for the R pulses to finally cross the line that separates enhancement from decoherence reduction. Notice also that the values of $\exp[-\Gamma_R(t_M, t_0)]$ for different realizations are not so spread and the standard deviations are narrower than in the high-temperature limit. In addition, the average over realizations is very close to the lower bound, to
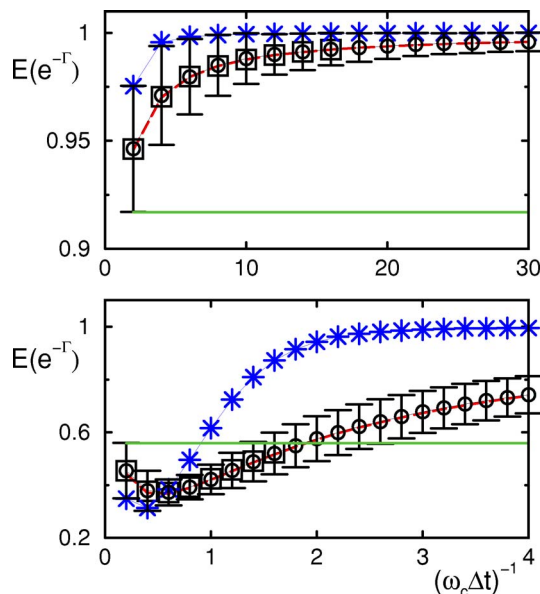

FIG. 11. (Color online) Decoherence rate for a low-temperature Ohmic bath, $T = 10^{-2} \omega_c$. Upper panel: $\omega_c t_f = 1$. Lower panel: $\omega_c t_f = 10$. (Green) solid line: no control. (Blue) stars: A protocol. (Black) circles: average over 10^3 realizations and respective standard deviations for the R protocol. (Black) squares: expectation value for the R protocol.
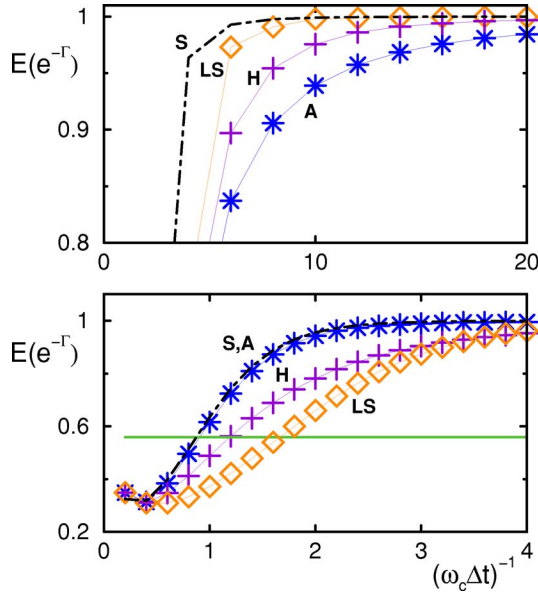
FIG. 12. (Color online) Decoherence rate. Upper panel: high-temperature Ohmic bath, $T = 10^2 \omega_c$, and $\omega_c t_f = 1$. Lower panel: low-temperature Ohmic bath, $T = 10^{-2} \omega_c$, and fixed time $\omega_c t_f = 10$. (Green) solid line: no control. (Blue) stars: A protocol. (Purple) plus: H protocol. (Orange) diamonds: LS scheme. (Black) dot-dashed line: S protocol. Average for the H protocol is taken over 10^3 realizations.

the point that they cannot be distinguished in the figure.

We now extend our comparison to the three remaining protocols of Fig. 1; see Fig. 12. We choose a high-temperature bath with $\omega_c t_f = 1$ (upper panel) (low temperature, in this case, leads to similar results) and a low-temperature bath with $\omega_c t_f = 10$ (lower panel). The S protocol shows the best performance, which is evident in the upper panel, but hardly perceptible in the lower one. Due to the different rearrangement of the time interval between pulses for this protocol, it does not correspond to any of the 2^M realizations of random pulses as considered here and represents a special scheme separated from the others. The performance of the LS protocol, which has half the number of π pulses used in the A protocol, turns out to be better in all cases of a high-temperature bath, but worse for a fully quantum bath with large $\omega_c t_f$. This explains why the H protocol, which combines symmetrization and randomness, also performs better than the A protocol in the high-temperature limit.

To summarize, in terms of performance, we have, in decreasing order, S, LS, H, A, and R protocols for high temperature and S, A, H, LS, and R protocols for low temperature once the number of pulses is sufficient to start slowing down decoherence. Different protocols become again, as expected, essentially equivalent in the limit $\Delta t \to 0$. For finite pulse separations, in the considered case of a time-independent Hamiltonian, it is always possible to identify a deterministic protocol showing the best performance. However, if a balance is sought between good performance and protocols minimizing the required number of pulses, then the H protocol again emerges as an interesting compromise. Note, in particular, that the latter outperforms the standard A protocol in some parameter regimes.

D. Randomized decoupling in the physical frame

We now investigate under which conditions decoherence suppression is attainable in the physical frame, when the system is subjected to randomized control. Because, in this frame, the qubit natural frequency plays an important role, random decoupling also depends on how small Δt can be made with respect to $\tau_0 = \omega_0^{-1}$.

The reduced density matrix is obtained following the same steps described so far, but in order to retain the effects of the system Hamiltonian, the transformation into the interaction picture is now done with respect to the environment Hamiltonian only—hence the superscript *IE*. Upon tracing over the environment degrees of freedom, we are left with the reduced density operator in the Schrödinger picture.

The unitary operator between pulses is

$$U^{IE}(t_{j+1}, t_j) = \exp\left(-i\frac{\omega_0}{2}\sigma_z \Delta t\right)$$
$$\times \exp\left\{\frac{\sigma_z}{2} \otimes \sum_k [\xi_k(\Delta t) b_k^\dagger e^{i\omega_k t_j} - \text{H.c.}]\right\}, \quad (63)$$

while at t_j it is given by

$$P_j^{IE} = \exp\left[-i\lambda_j \frac{\pi}{2} \sigma_x\right]. \quad (64)$$

By additionally moving to the logical frame we get

$$\tilde{U}^{IE}(t_M, t_0) = \exp\left[-i\frac{\omega_0}{2}\sigma_z \Delta t \sum_{j=0}^{M-1} \chi_j\right]$$
$$\times \exp\left\{\frac{\sigma_z}{2} \otimes \sum_k [b_k^\dagger e^{i\omega_k t_0} \eta_k^R(M, \Delta t) - \text{H.c.}]\right\}. \quad (65)$$

Tracing over the environment and taking the expectation over control realizations leads to the coherence element in the logical frame:

$$\mathbb{E}(\tilde{\rho}_{01}(t_M)) = \frac{\rho_{01}(t_0)}{2^{M-1}} \sum_{k=1}^{2^{M-1}} \cos[\Xi_{M-1}^{(k)} \omega_0 \Delta t] e^{-\Gamma_R^{(k)}(t_M, t_0)}, \quad (66)$$

where $\Xi_{M-1}^{(k)}$ is given by Eq. (44). Thus, in addition to the decoherence described as before by Eq. (58), we now have ensemble dephasing due to the fact that each realization carries a different phase factor proportional to ω_0.

The results for the ratios

$$F_1(t_M) = \frac{\mathbb{E}(\tilde{\rho}_{01}(t_M))}{\rho_{01}(t_0)} \quad \text{and} \quad F_2(t_M) = \frac{\mathbb{E}(\tilde{\rho}_{01}^I(t_M))}{\rho_{01}(t_0)} \quad (67)$$

in the logical and logical-IP frames for the system, respectively, are summarized in Fig. 13, where Δt is fixed and the system is observed at different times. Both a high-temperature and a low-temperature scenario are considered. The phase for each realization in the logical frame is mostly irrelevant when $\omega_0 \ll 1/\Delta t$. The outcomes of the average
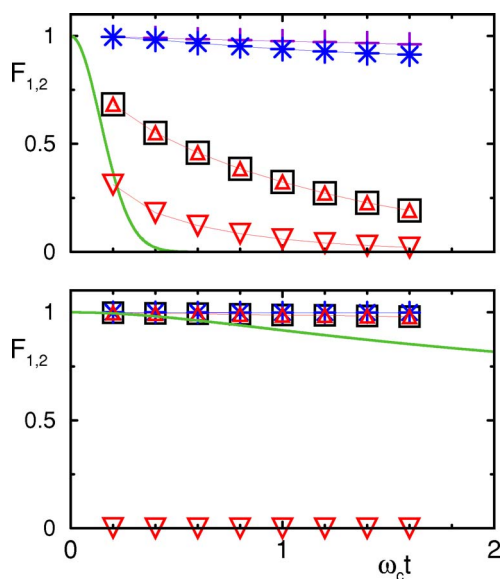
FIG. 13. (Color online) Ratios $F_1(t)$ and $F_2(t)$ in the logical and logical-IP frames, respectively. A fixed time interval $\Delta t = 1/(10\omega_c)$ is taken. Upper panel: high-temperature Ohmic bath, $T = 10^2\omega_c$. Lower panel: low-temperature Ohmic bath, $T = 10^{-2}\omega_c$. (Green) solid line: no control. (Blue) stars: A protocol. (Purple) plus: H protocol. (Black) squares: R protocol in the logical-IP frame. (Red) up triangles: R protocol in the logical frame with small frequency $\omega_0\Delta t = 10^{-3}$. (Red) down triangles: R protocol in the logical frame with large frequency $\omega_0\Delta t = \pi/2$. Average performed over all realizations.

over all realizations in both frames are then comparable, independently of the bath temperature. The situation changes dramatically when the spin-flip energy becomes large, the worst scenario corresponding to $\omega_0 = k\pi/(2\Delta t)$, with k odd. Here, because $\Xi_{M-1}^{(k)}$ is an even number, each realization makes a positive or a negative contribution to the average, which may therefore be very much reduced. Such destructive quantum interference is strongly dependent on the bath temperature.

Among all random pulse realizations, the most effective at suppressing decoherence are those belonging to the smaller ensemble of the H protocol. None of them carries a phase, so they always make large positive contributions to the total ensemble average. In a high-temperature bath, the realizations that can make negative contributions have often tiny values of $e^{-\Gamma_R(t_M,t_0)}$, which explains why even in the extreme case of $\omega_0 = k\pi/(2\Delta t)$ the R protocol can still lead to some decoherence reduction. In a low-temperature bath, on the other hand, decoherence is slower, and for the time considered here, the values of $e^{-\Gamma_R(t_M,t_0)}$ for all realizations are very close, which justifies their cancellation when $\omega_0 = k\pi/(2\Delta t)$.

In the physical frame, the average for the density matrix depends on the initial state of the system as

$$\mathbb{E}(\rho_{01}(t_M)) = \frac{\rho_{01}(t_0) + \rho_{10}(t_0)}{2^M} \sum_{k=1}^{2^{M-1}} \cos[\Xi_M^{(k)}\omega_0\Delta t]e^{-\Gamma_R^{(k)}(t_M,t_0)}.$$

As already discussed in Sec. III, the problem associated with population inversion may be avoided if a classical register is
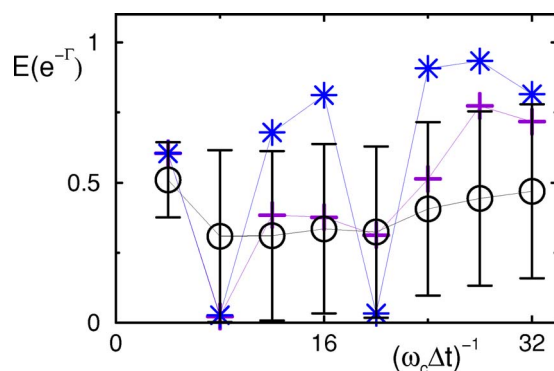

FIG. 14. (Color online) Decoherence rate for a high temperature Ohmic reservoir, $T = 10^2\omega_c$, with alternating couplings. (Blue) stars: A protocol. (Black) circles: R protocol. (Purple) plus: H protocol. The interval considered is $t_f = 1/\omega_c$. Averages taken over all possible realizations.

used to record the actual number of spin flips.

To summarize, two conditions need to be satisfied for the R protocol to become efficient in reducing decoherence: $\omega_c\Delta t \ll 1$ and also $\omega_0\Delta t \ll 1$. Notice, however, that when randomness and determinism are combined in a more elaborated protocol, such as the H protocol, no destructive interference due to ω_0 occurs. In addition, the hybrid scheme is still capable of outperforming the A protocol in appropriate regimes.

E. Time-dependent coupling Hamiltonian

As a final example, imagine that the coupling parameters $g_k(t)$ between the system and the environment are time dependent and let us for simplicity work again in the logical-IP frame. The total Hamiltonian is given by Eqs. (1) and (2) with $\omega_0(t) = \omega_0$ and $\mu = 1$. Two illustrative situations are considered: $g_k(t)$ changes sign after certain time intervals or it periodically oscillates in time.

1. Instantaneous sign changes

Suppose that $g_k(t) = g_k D(t)$, where

$$D(t) = (-1)^{\lfloor 10\omega_c t/3 \rfloor} \quad (68)$$

describes instantaneous sign changes of the coupling parameter after every interval $3/(10\omega_c)$. For a high-temperature bath and a fixed time $t_f = 1/\omega_c$, Fig. 14 shows that the results for the A protocol exhibit a drastic drop when $\Delta t = t_f/4$ and $\Delta t = t_f/10$. This is due to the fact that some of sign changes happen very close to or coincide with some of the π pulses of the deterministic sequence, canceling their effect. In contrast, the occurrence of spin flips in randomized schemes is irregular, so that the latter are more protected against such "resonances" and steadily recover coherence as Δt decreases, even though at a slower pace. Note that when dealing with the S or LS protocols, the same sort of recoil should be expected for different time dependences and different values of Δt.
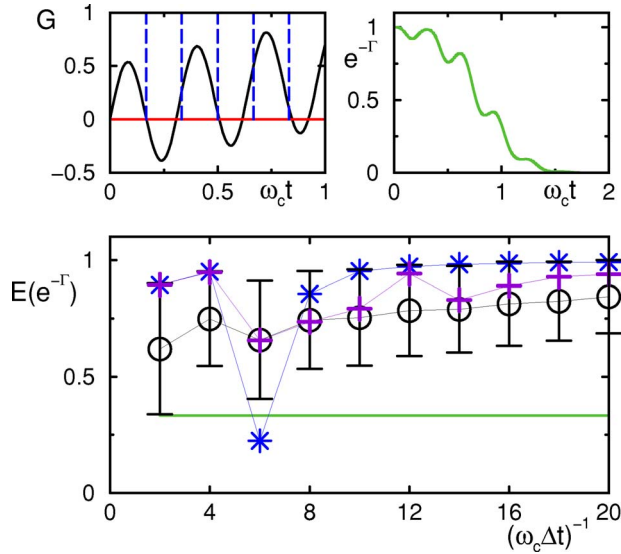
FIG. 15. (Color online) Upper left panel: function $G(t)=\cos(p\pi\omega_c t)\sin(q\pi\omega_c t)$, for $p=2.95$ and $q=3.25$. Upper right panel: decoherence rate in the absence of control. Lower panel: decoherence rate for a fixed time interval $\omega_c t_f=1$. A high-temperature Ohmic bath, $T=10^2\omega_c$, is considered. (Green) solid line: no control. (Blue) stars: A protocol. (Black) circles: R protocol. (Purple) plus: H protocol. Averages taken over 10^3 realizations. Standard deviations for the R protocol are shown.

2. Periodic modulation

Assume that the coupling parameter is given by $g_k(t)=g_k G(t)$, where $G(t)=\cos(p\pi\omega_c t)\sin(q\pi\omega_c t)$ and $|p-q|$ is small. This function has two superposed periodic behaviors, one with a long period and the other fast oscillating. The fast oscillations are shown in the left upper panel of Fig. 15.

We consider a high-temperature bath, $T=10^2\omega_c$. The right upper panel shows the qubit decoherence in the absence of pulses. The oscillations in the decay rate are related to the oscillations in the interaction strength between the system and bath. In the lower panel, we fix a time $t_f=1/\omega_c$ and compare the decoherence rate for the cases of absence of control, A, H, and R protocols. When $\Delta t=t_f/6$ the result for the A protocol suddenly becomes even worse than not acting on the system. Random pulses, on the contrary, do not show any significant recoil. The reason for the inefficiency of the A protocol when $M=6$ becomes evident from the left upper panel of Fig. 15. Vertical dashed lines indicate where the pulses occur. They mostly coincide with the instants where $G(t)$ also changes sign. For the LS protocol, similar unfavorable circumstances happen for different values of Δt and similar behaviors should be expected for other deterministic protocols and functions $g_k(t)$.

To summarize, the above examples again reinforce the idea of enhanced stability of randomized controls and suggest that randomization might represent a safer alternative in reducing decoherence when limited knowledge about the system-bath interaction is available.

VI. CONCLUSION

A. Summary

A quantitative comparison between deterministic and randomized control for the most elementary target system, consisting of a single (isolated or open) qubit, was developed in different frames. The main conclusions emerging from this study may be summarized as follows.

First, it is always possible to identify conditions under which purely random or hybrid schemes succeed at achieving the desired level of dynamical control. Frame considerations play an important role in specifying such conditions, satisfactory performance in a given frame being ultimately determined by a hierarchy of time scales associated with all the dynamical components in the relevant Hamiltonian. While all protocols become essentially equivalent in the limit of arbitrarily fast control, the behavior for finite pulse separation is rich and rather sensitive to the details of the underlying dynamics. As a drawback of pure random design, an ensemble average tends to introduce, in general, additional phase damping, which may be, however, circumvented by combining determinism and randomness within a hybrid design.

Second, for time-independent control settings in this simple system, it was always possible to identify a deterministic protocol with best performance. While deterministic schemes ensuring accurate averaging of a known interaction always exist in principle [1], such a conclusion remains to be verified under more general circumstances, in particular access to a *restricted* set of control operations. The hybrid protocol proved superior to the pure random schemes, as well as to standard asymmetric schemes in certain situations.

Third, for time-varying systems, randomized protocols typically allow for enhanced stability against parameter variations, which may severely hamper the performance of deterministic schemes. Pure random design tends to perform better than hybrid in this respect, both choices, however, improving over purely cyclic controls under appropriate conditions.

Overall, hybrid design emerges as a preferred strategy for merging advantageous features from different protocols, thereby allowing one to better compromise between conflicting needs.

B. Outlook

From a conceptual standpoint, it is intriguing to realize that complete suppression of decoherence remains possible, in principle, by purposefully introducing a probabilistic component in the underlying control and perhaps surprising to identify cases where this leads to improved efficiency over pure deterministic methods.

In a broader context, however, it is worth mentioning that the philosophy of recognizing a beneficial role of randomness in physical processes has a long history. Within NMR, the stochastic averaging of intermolecular interactions in gases and isotropic liquids due to random translational and reorientational motions may be thought of as a naturally occurring random self-decoupling process [1]. In spectroscopic applications of so-called stochastic NMR and stochastic

magnetic-resonance imaging [60], spin excitation via trains of weak rf pulses randomly modulated in amplitude, phase, and/or frequency is used to enhance decoupling efficiencies over a broader frequency bandwidth than attainable otherwise. Even more generally, the phenomenon of stochastic resonance [61,62] is paradigmatic in terms of pointing to a constructive role of noise in the transmission of physical signals. Within QIP, strategies aimed at taking advantage of noise and/or stochasticity have been considered in contexts ranging from quantum games [63] to quantum walks [64] and dissipation-assisted quantum computation [65], as well as specific coherent-control [66] and quantum simulation [67] scenarios. Yet another suggestive example is offered by the work of Prosen and Žnidarič, who have shown how static perturbations characterizing faulty gates may enhance the stability of quantum algorithms [68]. More recently, as mentioned, both pure random [38] and hybrid [39] active compensation schemes for static coherent errors have been proposed. While it is important to stress that none of the above applications stem from a general *control-theoretic framework* as developed in [36], it is still rewarding to fit such different examples within a unifying perspective.

Our present analysis should be regarded as a first step toward a better understanding and exploitation of the possibilities afforded by randomization for coherent and decoherent error control. As such, it should be expanded in several directions, including more realistic control systems and settings and fault-tolerance considerations. While we plan to report on that elsewhere, it is our hope that our work will stimulate fresh perspectives on further probing the interplay between the field of coherent quantum control and the world of randomness.

APPENDIX: CONTROL HAMILTONIAN

The control Hamiltonian is designed according to the intended modification of the target dynamics in a desired frame. Throughout this work, our goal has been to freeze the system evolution by removing any phase accumulated due to the unitary evolution, as well as avoiding nonunitary ensemble dephasing and decoherence. As clarified below, this requires the use of *identical π pulses in the physical frame*. This condition may be relaxed at the expense of no longer refocusing the unitary evolution.

Let the control of the system be achieved via the application of an external alternating field (e.g., a radio-frequency magnetic field),

$$H_c(t) = \sum_j H_c^{(j)}(t) = \sum_j V^{(j)}(t)\cos[\omega t + \varphi_j(t)]\sigma_x, \quad (A1)$$

where the carrier is tuned on resonance with the qubit central frequency, $\omega = \omega_0$. As described in the text, $V^{(j)}(t) = V[\Theta(t$

$-t_j) - \Theta(t-t_j-\tau)]$ and each pulse happens at t_j, having duration τ and amplitude V. Upon invoking the rotating-wave approximation (RWA), hence neglecting the counterrotating terms $\sigma_-\exp\{-i[\omega_0 t + \varphi_j(t)]\}$ and $\sigma_+\exp\{i[\omega_0 t + \varphi_j(t)]\}$ in Eq. (A1), the control Hamiltonian given in the main text is found. The function $\varphi_j(t)$ characterizes the phase properties of the pulses we deal with. We compare two relevant possibilities.

(i) $\varphi_j(t) = -\omega_0 t_j$ for each j: This means that the pulses are identical in the physical frame, as used in this work.

(ii) $\varphi_j(t) = 0$ for all j: This means that the pulses are identical in the physical frame only if separated in time by a multiple of 2π.

The propagator corresponding to the above choices may be in general obtained by seeking a transformation which removes the time dependence of $H_c^{(j)}(t)$ within each pulse. A transformation to an *absolute* frame rotating with the carrier frequency, which on resonance is identical with the interaction picture, leads to

$$H_c^{I(j)}(t) = \exp[i\omega_0 t\sigma_z/2]H_c^{(j)}(t)\exp[-i\omega_0 t\sigma_z/2]$$

$$= V^{(j)}(t)\exp\left[-i\frac{\varphi_j(t)}{2}\sigma_z\right]\sigma_x\exp\left[i\frac{\varphi_j(t)}{2}\sigma_z\right].$$

Thus, the choice $\varphi_j(t) = 0$ corresponds to pulses which are translationally invariant in time in this frame. In case (i), the above transformation does not remove time dependence, which would instead be accomplished by moving to a *relative* rotating frame via a rotation $U_z(t-t_j) = \exp[i\omega_0(t-t_j)\sigma_z/2]$. From the above expression, the interaction-picture propagators for an instantaneous π pulse applied at t_j are found, respectively, as

$$\text{(i)} \quad P_j^I = \exp\left[i\frac{\omega_0 t_j}{2}\sigma_z\right]\exp\left[-i\frac{\pi}{2}\sigma_x\right]\exp\left[-i\frac{\omega_0 t_j}{2}\sigma_z\right],$$

$$\text{(ii)} \quad P_j^I = \exp\left[-i\frac{\pi}{2}\sigma_x\right].$$

We can then return to the Schrödinger picture using the relation

$$P_j = \exp[-i\omega_0 t_j\sigma_z/2]P_j^I\exp[i\omega_0 t_j\sigma_z/2],$$

leading to the propagators

$$\text{(i)} \ P_j = \exp\left[-i\frac{\pi}{2}\sigma_x\right],$$

$$\text{(ii)} \ P_j = \exp\left[-i\frac{\omega_0 t_j}{2}\sigma_z\right]\exp\left[-i\frac{\pi}{2}\sigma_x\right]\exp\left[i\frac{\omega_0 t_j}{2}\sigma_z\right].$$
$$(A2)$$

Thus, pulses with $\varphi_j(t) = -\omega_0 t_j$ are confirmed to be translationally invariant in time in the physical frame, as directly clear from the dependence $\omega_0(t-t_j)$ in Eq. (A1).

The difference between the two choices to the control purposes becomes evident by considering the A protocol on the isolated qubit. From Eqs. (A2), the propagators

$U(t_2,t_0) = P_2 U_0(t_2,t_1) P_1 U_0(t_1,t_0)$ in the physical frame are, respectively,

$$\text{(i)} \ U(t_2,t_0) = \mathbb{1},$$

$$\text{(ii)} \ U(t_2,t_0) = -\exp[-i\omega_0(t_2-t_1)\sigma_z], \qquad (A3)$$

which leads to the conclusion that refocusing in the physical frame may only be achieved with identical pulses—that is, if $\varphi_j(t) = \omega_0 t_j$. Clearly, for the choice $\varphi_j(t) = 0$, the accumulated phase may only be disregarded in the frame rotating with the frequency ω_0. Both choices are equally useful if decoherence suppression becomes the primary objective in the open system case.

[1] U. Haeberlen, *High Resolution NMR in Solids: Selective Averaging* (Academic Press, New York, 1976).
[2] R. R. Ernst, G. Bodenhausen, and A. Wokaun, *Principles of Nuclear Magnetic Resonance in One and Two Dimensions* (Oxford University Press, Oxford, 1994).
[3] P. W. Brumer and M. Shapiro, *Principles of the Quantum Control of Molecular Processes* (Wiley & Sons, New York, 2003).
[4] M. A. Nielsen and I. L. Chuang, *Quantum Computation and Quantum Information* (Cambridge University Press, Cambridge, UK, 2000).
[5] See e.g. http:qist.lanl.gov/qcomp-map.shtml for an up-to-date overview of existing approaches to QIP and a comparative analysis of their merits and weaknesses.
[6] U. Haeberlen and J. S. Waugh, Phys. Rev. **175**, 453 (1968).
[7] E. L. Hahn, Phys. Rev. **80**, 580 (1950).
[8] H. Y. Carr and E. M. Purcell, Phys. Rev. **94**, 630 (1954).
[9] L. Viola and S. Lloyd, Phys. Rev. A **58**, 2733 (1998).
[10] L. Viola, E. Knill, and S. Lloyd, Phys. Rev. Lett. **82**, 2417 (1999); L. Viola and E. Knill, *ibid.* **90**, 037901 (2003); L. Viola, Phys. Rev. A **66**, 012307 (2002).
[11] P. Zanardi, Phys. Lett. A **258**, 77 (1999).
[12] M. S. Byrd and D. A. Lidar, Quantum Inf. Process. **1**, 19 (2002).
[13] F. Ticozzi and A. Ferrante, in *Proceedings of the 44th IEEE Conference on Decision and Control* (in press).
[14] L. Viola and E. Knill, Phys. Rev. Lett. **90**, 037901 (2003).
[15] K. Khodjasteh and D. A. Lidar, Phys. Rev. Lett. **95**, 180501 (2005).
[16] J. A. Jones and E. Knill, J. Magn. Reson., Ser. A **141**, 322 (1999).
[17] M. Stollsteimer and G. Mahler, Phys. Rev. A **64**, 052301 (2001).
[18] D. Leung, J. Mod. Opt. **49**, 1199 (2002).
[19] M. Rötteler and P. Wocjan, e-print quant-ph/0409135; P. Wocjan, e-print quant-ph/0410107.
[20] P. Facchi, D. A. Lidar, and S. Pascazio, Phys. Rev. A **69**, 032314 (2004); P. Facchi, S. Tasaki, S. Pascazio, H. Nakazato, A. Tokuse, and D. A. Lidar, Phys. Rev. A **71**, 022302 (2005).
[21] C. Search and P. R. Berman, Phys. Rev. Lett. **85**, 2272 (2000);

Phys. Rev. A **62**, 053405 (2000).
[22] K. Shiokawa and D. A. Lidar, Phys. Rev. A **69**, 030302(R) (2004).
[23] H. Gutmann, F. K. Wilhelm, W. M. Kaminsky, and S. Lloyd, Phys. Rev. A **71**, 020302(R) (2005).
[24] G. Falci, A. D'Arrigo, A. Mastellone, and E. Paladino, Phys. Rev. A **70**, 040101(R) (2004).
[25] L. Faoro and L. Viola, Phys. Rev. Lett. **92**, 117905 (2004).
[26] H. Gutmann, F. K. Wilhelm, W. M. Kaminsky, and S. Lloyd, Quantum Inf. Process. **3**, 247 (2004).
[27] D. Vitali and P. Tombesi, Phys. Rev. A **59**, 4178 (1999); **65**, 012305 (2002).
[28] D. A. Lidar and L.-A. Wu, Phys. Rev. A **67**, 032313 (2003).
[29] D. A. Lidar and L.-A. Wu, Phys. Rev. Lett. **88**, 017905 (2002); L.-A. Wu and D. A. Lidar, *ibid.* **88**, 207902 (2002); M. S. Byrd and D. A. Lidar, *ibid.* **89**, 047901 (2002).
[30] A. J. Berglund, e-print quant-ph/0010001.
[31] D. G. Cory *et al.*, Fortschr. Phys. **48**, 875 (2000).
[32] N. Boulant, M. A. Pravia, E. M. Fortunato, T. F. Havel, and D. G. Cory, Quantum Inf. Process. **1**, 135 (2002).
[33] Y. Nakamura, Y. A. Pashkin, T. Yamamoto, and J. S. Tsai, Phys. Rev. Lett. **88**, 047901 (2002).
[34] I. Chiorescu, Y. Nakamura, C. J. P. M. Harmans, and J. E. Mooij, Science **299**, 1871 (2003).
[35] E. Fraval, M. J. Sellars, and J. J. Longdell, Phys. Rev. Lett. **95**, 030506 (2005).
[36] L. Viola and E. Knill, Phys. Rev. Lett. **94**, 060502 (2005).
[37] L. Viola, in *Proceedings of the 44th IEEE Conference on Decision and Control* (in press).
[38] O. Kern, G. Alber, and D. L. Shepelyansky, Eur. Phys. J. D **32**, 153 (2005).
[39] O. Kern and G. Alber, e-print quant-ph/0506038.
[40] M. Palma, K.-A. Suominen, and A. K. Ekert, Proc. R. Soc. London, Ser. A **452**, 567 (1996).
[41] H.-P. Breuer and F. Petruccione, *The Theory of Open Quantum Systems* (Oxford University Press, Oxford, 2002).
[42] It is worth noting that $(1/|\mathcal{G}|)\Sigma_{g\in\mathcal{G}}\Sigma(\cdot)$ corresponds to integration according to the invariant Haar measure on $\mathcal{G}$ in the discrete case considered here.

[43] S. Gheorghiu-Svirschevski, Phys. Rev. A **66**, 032101 (2002).

[44] Note that the first pulse is assumed to occur at t_1, but the cyclicity condition with the consequent phase removal is equally satisfied if we start pulsing the system at the initial time t_0. In this case, however, the last pulse occurs at t_{M-1}. The qubit evolves freely from t_{M-1} to t_M, where it should then be observed.

[45] The $*$ subscript is meant to stress the purely statistical origin of such a damping factor, somewhat reminiscent of the T_2^* dephasing time resulting from sample-to-sample variations in ensemble measurements.

[46] E. Mansfield, *Basic Statistics with Applications* (Springer-Verlag, New York, 1986).

[47] M. B. Weissman, Rev. Mod. Phys. **60**, 537 (1988).

[48] W. H. Press, Astrophys. **7**, 103 (1978).

[49] R. F. Voss, Phys. Rev. Lett. **68**, 3805 (1992).

[50] Y. Makhlin, G. Schön, and A. Shnirman, Rev. Mod. Phys. **73**, 357 (2001).

[51] E. Paladino, L. Faoro, G. Falci, and R. Fazio, Phys. Rev. Lett. **88**, 228304 (2002).

[52] T. Itakura and Y. Tokura, Phys. Rev. B **67**, 195320 (2003).

[53] Y. M. Galperin, B. L. Altshuler, and D. V. Shantsev, e-print cond-mat/0312490, also in *Fundamental Problems of Mesoscopic Physics*, edited by I. V. Lerner *et al.* (Kluwer Academic, Dordrecht, 2004).

[54] C. T. Rogers and R. A. Buhrman, Phys. Rev. Lett. **53**, 1272 (1984).

[55] R. T. Wakai and D. J. Van Harlingen, Phys. Rev. Lett. **58**, 1687 (1987).

[56] M. Dykman, Sov. J. Low Temp. Phys. **5**, 89 (1979).

[57] G. Gordon, G. Kurizki, A. G. Kofman, and S. Pellegrin, Quantum Inf. Comput. **5**, 285 (2005).

[58] D. Vitali and P. Tombesi, Phys. Rev. A **59**, 4178 (1999).

[59] The standard deviation considered here is a measure of how spread the results for different realizations are. It is the square root of the unbiased variance s_{N-1}^2, computed as

$$s_{N-1}^2 \equiv \frac{1}{N-1} \sum_{i=1}^{N} (x_i - \bar{x})^2,$$

where $\bar{x}$ is the sample mean, x_i corresponds to the different sample data, and N is the total number of data. Instead, the standard deviation mentioned in Sec. III is a measure of how spread the average obtained from a sample of the ensemble (sample mean/average value) is with respect to the average obtained from the full ensemble (expected value). It was used to infer the dependence of the sample size on the interval between pulses.

[60] R. R. Ernst and H. Primas, Helv. Phys. Acta **36**, 583 (1963); R. R. Ernst, J. Chem. Phys. **45**, 3845 (1966); B. Blümich and D. Ziessow, J. Magn. Reson. (1969-1992) **46**, 385 (1982).

[61] L. Gammaitoni, P. Hänggi, P. Jung, and F. Marchesoni, Rev. Mod. Phys. **70**, 223 (1998).

[62] L. Viola, E. M. Fortunato, S. Lloyd, C.-H. Tseng, and D. G. Cory, Phys. Rev. Lett. **84**, 5466 (2000).

[63] C. F. Lee and N. F. Johnson, Phys. Lett. A **301**, 343 (2002).

[64] V. Kendon and B. Tregenna, Phys. Rev. A **67**, 042315 (2003).

[65] A. Beige, D. Braun, B. Tregenna, and P. L. Knight, Phys. Rev. Lett. **85**, 1762 (2000); A. Beige, Inst. Phys. Conf. Ser. **173**, 35 (2003).

[66] S. Mancini, D. Vitali, P. Tombesi, and R. Bonifacio, Europhys. Lett. **60**, 498 (2002).

[67] M. J. Bremner, J. L. Dodd, M. A. Nielsen, and D. Bacon, Phys. Rev. A **69**, 012313 (2004).

[68] T. Prosen and M. Žnidarič, J. Phys. A **34**, L681 (2001); **35**, 1455 (2002).